Chemical Geology 288 (2011) 67–85

Contents lists available at ScienceDirect

Chemical Geology

journal homepage: www.elsevier.com/locate/chemgeo

Regional variations in the chemical and helium–carbon isotope composition of geothermal fluids across Tunisia

E. Fourré [a,*], R. Di Napoli [b], A. Aiuppa [b,c], F. Parello [b], E. Gaubi [d], P. Jean-Baptiste [a], P. Allard [e], S. Calabrese [b], A. Ben Mamou [d]

[a] LSCE, CEA-Saclay, Gif-sur-Yvette, France
[b] DiSTeM, Università di Palermo, Italy
[c] Istituto Nazionale di Geofisica e Vulcanologia, Sezione di Palermo, Italy, Italy
[d] Laboratoire Ressources Minérales et Environnement, Univ. Tunis El-Manar, Tunisia
[e] IPGP, Paris, France

ARTICLE INFO

Article history:
Received 17 January 2011
Received in revised form 19 May 2011
Accepted 7 July 2011
Available online 19 July 2011

Keywords:
Tunisia
Helium isotopes
Carbon isotopes
Geothermal fluids
Groundwaters
Thermal springs

ABSTRACT

Tunisia has numerous thermo-mineral springs. Previous studies have shown that their chemical composition and occurrence are strongly influenced by the regional geology. However little work has been done so far to study the isotopic composition of volatiles associated with these geothermal manifestations. Here, we report on the results of an extensive survey of both natural hot springs and production wells across Tunisia, aimed at investigating the spatial distribution of thermal fluids' geochemical characteristics and He–C isotopic composition. The chemistry of the analyzed samples highlights the heterogeneity of the water mineralization processes in Tunisia, as a consequence of the complex geological and tectonic setting of the country. In terms of chemical composition, we are able to conclude, however, that dissolution of halite and gypsum plays a key control on groundwater chemistry. Helium and carbon isotope systematics confirm the prevalently crustal origin of the volatiles interacting with the aquifer systems, consistent with the absence of any recent magmatism. Most samples are characterized by crustal-type helium ($^3He/^4He$ in the range 0.02 Ra–0.4 Ra) associated with a CO_2 predominantly metamorphic in origin (with the exception of the Saharan platform where the carbon content is low and mostly organically-derived). In Eastern Tunisia, however, a few samples have He–C isotope compositions which suggest (at least partial) mantle derivation of the dissolved gas phase : the $^3He/^4He$ ratio reaches 2.4 Ra (corresponding to 30% of mantle-derived helium) at the Ain Garci site, a CO_2 rich mineral spring located some 30 km south of the city of Zaghouan. This mantle signature is consistent with the fact that the Pelagian Block, to which Eastern Tunisia belongs, has been deeply affected by extensional and transtensional tectonics since the opening of the Tethys, a process which is still ongoing in the Sicily channel (Pantelleria Rift). As a whole however, our results show that the Italian mantle gas anomaly only marginally extends to Northwestern Africa.

1. Introduction

Tectonically- and seismically-active regions of the world have long been known for being sites of widespread release of deep-rising fluids and associated volatiles (Irwin and Barnes, 1980). In the central Mediterranean for instance, studies of the Italian peninsula have shown that, in addition to the huge gas emissions from active volcanism (Allard et al., 1991; Aiuppa et al., 2008), large amounts of volatiles (e.g., $>2\cdot10^{11}$ mol/year of CO_2; Chiodini et al., 2004, 2008) are also released in diffuse form through the tectonically active Tyrrhenian segment of the country. Such volatile degassing occurs in either diffuse form (through regional aquifers), or diffuse soil degassing, or in localized (spot) manifestations, either cold or hot (fumaroles, hot springs, etc.). The question therefore arises whether, and to what extent, such degassing pattern also extends to nearby north-western Africa, an area which has undergone similarly complex tectonic evolution since the Mesozoic.

Tunisia, in particular, has numerous thermo-mineral springs, the majority of which are used for public baths (*hammam*), swimming pools, and for medical treatments provided by thermal establishments. Previous studies (Meddeb, 1993; Sadki, 1998) have shown that location and chemical composition of these thermal manifestations are strongly influenced by the regional geology. However, while geology and tectonism in Tunisia have long been a subject of interest, little work has been conducted so far to investigate the isotopic composition of volatiles associated with these geothermal manifestations, and their relation with the geological and structural framework of Tunisia.

* Corresponding author.
E-mail address: Elise.Fourre@lsce.ipsl.fr (E. Fourré).

0009-2541/$ – see front matter © 2011 Elsevier B.V. All rights reserved.
doi:10.1016/j.chemgeo.2011.07.003

Many studies have demonstrated that the characterization of the He–CO_2 relative abundances and isotopic compositions in geothermal manifestations can valuably assist in constraining the origin of the fluids (Marty and Jambon, 1987; Griesshaber et al., 1992; Lollar et al., 1997; Hulston et al., 2001; de Leeuw et al., 2007; Mutlu et al., 2008; Lollar and Ballentine, 2009; Mata et al., 2010). In this respect, because they vary by more than three orders of magnitude in terrestrial samples, helium isotopes are particularly good indicators of both the extent of mantle-derived contributions to crustal fluids and the rate of mantle degassing through the crust (Ballentine et al., 1991; Marty et al., 1992; Ballentine et al., 2002; Güleç et al., 2002; Kipfer et al., 2002 and references therein). This results from the distinct origins of ^{3}He (essentially primordial) and ^{4}He (produced by the radioactive decay of U and Th) and their contrasted proportions in Earth's reservoirs. When referred to the atmospheric ratio ($R_a = 1.38 \times 10^{-6}$), typical ^{3}He/^{4}He ratios vary from <0.05 R_a in the continental crust to 8 ± 1 R_a on average in the upper mantle, and up to ~40–50 R_a in products of plume-related ocean islands, such as Hawaii and Iceland (Marty et al., 1991, 1996; Ballentine and Burnard, 2002; Graham, 2002; Hilton et al., 2002; Stuart et al., 2003). Spatial variations of the ^{3}He/^{4}He ratios can thus be used to identify contemporary magmatic activity and/or tectonic processes that may facilitate the transport of mantle volatiles to shallow crustal levels (Polyak et al., 2000; Ballentine et al., 2002; Caracausi et al., 2005; Pik and Marty, 2009) and provide valuable information about regional tectonic environments. The application of the above "isotopic approach" to Italian gas discharges for instance, has revealed a complex scenario in which an heterogeneous (variably metasomatized) mantle, and gas production in the crust, both contribute to the source of the surface gas anomaly (e.g., Chiodini et al., 2000, 2004; Parello et al., 2000; Martelli et al., 2004, 2008).

Here, we report on the results of a survey, carried out in 2006 and 2009, of both production wells and natural hot springs across Tunisia. A total of 43 springs and wells were sampled for carbon and helium isotope geochemistry to map the spatial distribution of $\delta^{13}C_{TDIC}$ (TDIC stands for Total Dissolved Inorganic Carbon) and ^{3}He/^{4}He ratios. In addition to water samples, gas samples were also collected and analyzed for helium isotopes whenever gas bubbles were present. At each site, samples were also taken for chemical analysis and stable isotope geochemistry (O, H). The aim of this work is to determine helium and associated carbon isotopic composition of the main geothermal areas of Tunisia in order to gain insights into the subsurface physical and chemical processes determining the geochemistry of Tunisian hydrothermal manifestations and their links with the complex neotectonic framework of the country.

2. The study area

2.1. Geological and tectonic settings

Tunisia belongs to the North African margin (Fig. 1). It occupies a peculiar position at the boundary between the stable Precambrian Saharan domain and the younger and deformed Atlasic domain. A complex tectonic evolution, resulting from interactions between the African and European plates, has affected Tunisia since the Late Permian, at the beginning of Pangea breakup, and until the Cenozoic Alpine orogeny of the Maghrebide chain (Bouaziz et al., 2002). As a result, the geology of Tunisia is of remarkable complexity.

Three main structural domains can be identified in Tunisia : the Saharan, the Atlasic and the Eastern domains (Fig. 1). The Saharan domain, in southern Tunisia, forms a stable tabular zone which consists of a granitic and metamorphic basement (Laaridhi-Ouazaa, 1994), overlain by a thin and relatively undeformed sequence of Paleozoic sandstones and carbonates, and Mesozoic evaporites (Ben Ferjani et al., 1990). In its southernmost part, the Saharan plateau is covered by the dunes of the Grand Erg Oriental, while in the north, the

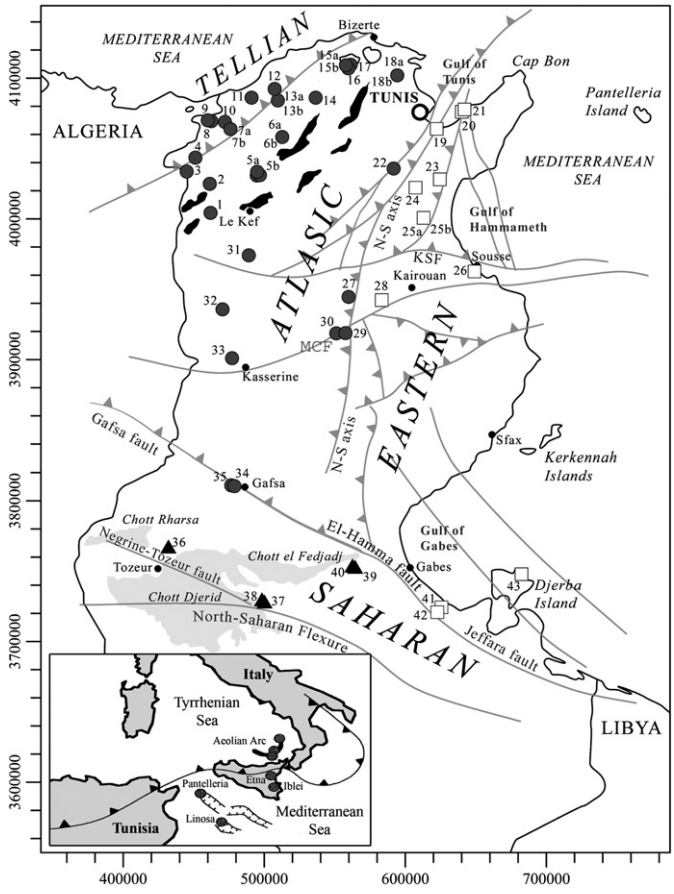

Fig. 1. Simplified structural map of Tunisia, showing its main structural domains (see Section 2): the *Saharan domain*, the *Atlasic domain*, and the *Eastern domain*. The Tellian sector is identified as the NW portion of the Atlasic domain. NE–SW trending Triassic "diapir zone", from Tunis to Le Kef, is marked in black. Sampling sites (numbered as in Table 1) are shown with different symbols for samples collected in the different geographical districts : samples from the Atlasic domain are represented by circles, from the Eastern domain by squares, and from the Saharan domain by triangles. The small inset puts Northern Tunisia in a broader geodynamic context, and shows the collisional boundary between African and European plates, as well as the sites of active volcanism in Sicily and Eolian Islands (black dots).
Modified from Khomsi et al. (2007).

Chotts region comprised between the North Saharan Flexure (Gabtni et al., 2005) and the Gafsa-Jeffara fault system separates this Saharan domain from the thick and folded sedimentary cover of the Atlasic domain (Fig. 1). To the north of the Saharan Platform, the Atlasic domain, with the meridional, central and northern Atlas, occupies most of central Tunisia. It consists of a complex sequence of dominantly SE-verging tectonic depressions and uplifts that developed during the late Cretaceous collision between the African and European plates. It includes the main mountains and ranges of Tunisia, which were formed in a compressive context since the Late Eocene. This domain extends up to the northern coast of Tunisia, while, on its eastern side, it is limited by the North–South Axis (Fig. 1), a major structural lineament trending N–S from the Gulf of Tunis and corresponding to a deep fault system oriented N–S (Burollet, 1956). Thick and well-deformed series of Cretaceous and Tertiary sediments, formed during the Atlas orogeny, make up the Atlasic domain. Marine carbonates with significant fossiliferous content and secondary dolomite, clay and gypsum formations, outcrop in the southernmost part of the Atlasic domain (Gafsa zone, and Kasserine "island"). Further to the north, the Atlasic domain grades to deep marine basin deposits, named "Tunisian Trough", consisting of Cretaceous and Tertiary shales and carbonate formations. In this area, NE–SW

trending folds and fractures give rise to widespread extrusions of evaporites from the Triassic basement (Perthuisot, 1978; Mlayah et al., 2009); finally giving rise to a ~1000 m thick "diapir zone" (Fig. 1) mainly composed of gypsum and anhydrite, with interbedded clays and thin dolomite layers. This evaporitic sequence, which was deposited during the Late Triassic–Liassic in an epicontinental domain, thickens towards the north, and grades to evaporitic series including abundant halite (Ben Ferjani et al., 1990). To the extreme northwest, the Tellian sector (Fig. 1) occupies the eastern part of the "Maghrebides" fold-thrust belt. It corresponds to a "nappe" domain (Ben Ferjani et al., 1990) made of several geological units displaced southeastward by the tectonic activity (Rouvier, 1977). It was formed during the Late Miocene major orogeny, and its uppermost part is composed of thick (3000–4000 m) series of sandstones and shales belonging to the Oligo-Miocene Numidian Flysch units (Rouvier, 1977). The recent tectonic events in the area are thought to be responsible for its relatively high geothermal gradient (8–9 °C/100 m) and associated high density of thermal manifestations (Meddeb, 1993).

The Eastern domain (Fig. 1) constitutes the young eastern continental margin of Tunisia. It belongs to the Pelagian block, which extends from Tunisia to Sicily, and is characterized by strong extensional tectonics (Pantelleria rift zone) and present-day magmatic activity. Salt pans (sebkhas) and plains (e.g. Kairouan and Sfax plains) characterize this flat area, which was protected from the Atlasic compression by the N–S axis. Since late Cretaceous times, it has followed its own geodynamic evolution and is affected by important tectonic activity of transtensional and transpressional N–S and E–W deep-seated faults, giving rise to a mosaic of Mesozoic and Cenozoic grabens, horsts, platforms and folds (Bédir, 1995, 1999)

Basic and acidic igneous rocks are widespread all over Tunisia (Ben Ferjani et al., 1990), testifying that volcanic activity has periodically occurred since the Jurassic–Early Cretaceous. The mafic volcanic products are related to the Mio-Pliocene extensional phase, while the more sialic products can be ascribed to shallow crust melting processes during the Miocene compression (Mauduit, 1978).

2.2. Hydrogeological setting

The southern Tunisia deep groundwater system is part of the "Continental Intercalaire" aquifer (CI), one of the largest confined aquifers in the world (Castany, 1982), comparable in scale to the Great Artesian basin of Australia. It covers an area of ~600,000 km^2 from western Algeria to the Lybian desert and, from north to south, from the Saharan Atlas to the Tassili. It is divided into two sub-basins by the M'zab dorsal : the eastern sub-basin flows towards its natural discharge area of the Tunisian Chotts region and of the Gulf of Gabès, where its mixes with the local Djeffara aquifer. The CI consists of several water horizons with strong artesian pressure (5–25 bars), high temperatures (65–75 °C) and prevalent Na–SO_4–Cl composition (Edmunds et al., 2003). The groundwater reservoir of the CI is hosted by the continental formations of the Lower Cretaceous (Neocomian, Barremian, Aptian and Albian). The geology of the CI has been described by Cornet (1964), Bishop (1975) and Castany (1982); the most significant formations include limestones, dolomites, clays, sands, and gypsum-bearing evaporites (Bouri et al., 2008).

Elsewhere in Tunisia, groundwater origin is much more local. Rainwaters infiltrate into the crust, dissolve salts, and warm up under the effect of the geothermal heat flux. Although water emergences are found in all types of sedimentary terrains from the Lias to the Quaternary, most of them coincide with the permeable formations of the upper Eocene and the Oligocene, often in association with tectonic accidents and deep fractures (Jellouli, 2002).

3. Sampling and methods

A first sampling campaign for isotopic and geochemical analyses was performed during September 2006. A second campaign took place in October 2009 to complete the initial data set, including seven sites already sampled in 2006. In addition to water samples, gas samples were also collected for helium isotopes whenever gas bubbles were present (five sites). Location of the sampling points is given in Table 1, and displayed on the schematic map of Tunisia (Fig. 1).

Results of analytical determinations are listed in Tables 1 and 2. Discharge temperature, pH, Eh and conductivity were measured in the field using portable instruments. Samples for laboratory chemical analyses were collected and stored in LDPE (low density polyethylene) bottles in order to measure major and minor ion concentrations. Analytical determinations were carried out at Instituto Nazionale di Geofisica e Vulcanologia (INGV), sezione di Palermo. The HCO_3 content was determined by volumetric titration with HCl 0.1 N as titrating reagent and methylorange as indicator. Chemical analyses of major constituents were performed by ion-chromatography (Dionex DX120) using specific columns for anions (AS14A) and cations (CS12A). Filtered (0.45 μm) and acidified (to pH = 2 with ultra-pure HNO_3) samples were used to determine Na, K, Mg and Ca concentrations, while anion species (F, Cl, Br, NO_3, SO_4) were determined on untreated samples. The quality of sample analysis was assessed from ionic balance : all samples exhibited imbalances below ±3%.

The composition of dissolved gasses (O_2, N_2, CO_2, CH_4, H_2 and CO) was determined (also at INGV sezione di Palermo) following the procedures described in Capasso and Inguaggiato (1998) and Capasso et al. (2000), using a Perkin Elmer Auto system XLClarus 500 gas chromatographer equipped with Carboxen 1000 columns. A thermal conductivity detector (HWD) was used to measure the concentrations of H_2, O_2, N_2 and CO_2, while CH_4 and CO were determined by a flame ionization detector (FID). In Table 2, we report the volumetric percentages (% vol.) in the dry gas phase of the various gaseous species in equilibrium with each collected water sample, calculated at the sampling temperature according to Capasso and Inguaggiato (1998).

The isotopic composition of Total Dissolved Inorganic Carbon (TDIC) was determined at INGV sezione di Palermo, after purification of the stripped CO_2, using a Finningan Delta Plus mass spectrometer. The isotopic value of $\delta^{13}C_{TDIC}$ (see Table 1), calculated according to the method proposed by Favara et al. (2002), are expressed as δ ‰ vs. PDB, with an accuracy of ±0.1‰.

Hydrogen and oxygen isotope analyses were performed at LSCE (Saclay) using the uranium reduction and the CO_2 equilibration techniques, respectively. The experimental precision of the isotopic analysis is 0.8‰ for δD and 0.05‰ for $\delta^{18}O$ (Stievenard et al., 1994; Bourg et al., 2001).

Water samples for helium isotopes were collected in standard refrigeration grade 3/8″ copper tubes equipped with metal clamps at both ends. The tubes were flushed with the water prior to closure using either the natural water flow or a perilstaltic pump connected with Tygon tubing. When present, gas bubbles in water were also collected in copper tubes using an inverted funnel. The helium and neon isotopic analyses were carried out at LSCE (Saclay) with a MAP-215 mass spectrometer using standard procedures (Jean-Baptiste et al., 1992). Gas samples in copper tubes were directly connected to the high-vacuum inlet system of the mass spectrometer. Helium and neon dissolved in the water samples were first extracted under vacuum into sealed glass tubes (Jean-Baptiste et al., 1992). Typical ^{4}He and ^{20}Ne blanks are 5×10^{-10} and 3×10^{-10} cm^3 STP for the mass spectrometer inlet, and 2×10^{-9} and 1×10^{-9} cm^3 STP for the extraction system, respectively. The accuracy is ±1% for helium and neon concentrations in both water and gas samples. The analytical

Table 1
Sample details including sampling location, water chemistry and stable isotopes.

Sample	Site name (location N,E)	Sampling date	T	pH	cond.	Eh	Na	K	Mg	Ca	F	Cl	Br	NO_3	SO_4	Alk	TDS	$\delta^{18}O$	δD	SI	SI	SI
			°C		mS/cm	mV	meq/l	meq/l	meq/l	meq/l	meq/l	meq/l	meq/l	meq/l	meq/l	meq/l	mg/l	‰	‰	halite	gypsum	calcite
Atlasic samples																						
1	H. Mallègue 4004342, 461841	13/10/2006	41.8	6.64	20.7	−48	1.17E+02	0.84	6.85	14.7	0.002	1.17E+02	b.d.l.	b.d.l.	8.67	8.8	8.19E+03	−6.75	−42.0	−3.73	−1.59	0.23
2	H. Bezzaz 4025220, 461206	12/10/2006	48.5	6.53	33.5	49.5	1.68E+02	1.60	9.57	23.1	0.002	1.81E+02	b.d.l.	b.d.l.	18.1	16.2	1.28E+04	−6.94	−40.1	−3.43	−1.22	0.58
3	H. Ouchtata 4033459, 444894	29/09/2009	42.9	7.04	2.33	−180	1.54E+01	0.15	0.34	1.37	0.056	4.98E+00	b.d.l.	0.03	0.81	11.3	1.30E+03	−7.14	−36.8	−5.86	−2.52	−0.03
4	H. Ali Daoua 4043096, 450931	12/10/2006	39.5	6.39	99.7	93	7.07E+02	3.52	20.0	51.0	0.002	7.32E+02	b.d.l.	b.d.l.	58.7	10.6	4.71E+04	−6.52	−33.6	−2.28	−0.83	0.23
5a	H. Biadha 4031101, 495048	10/10/2006	40.6	6.07	94	−107	6.80E+02	5.56	28.7	64.0	0.002	6.75E+02	b.d.l.	3.67	79.4	26.2	4.71E+04	−6.85	−37.5	−2.34	−0.62	0.4
5b	H. Biadha 4031101, 495048	29/09/2009	40.6	6.06	48.5	−52	7.73E+02	4.85	29.9	80.2	n.d.	8.00E+02	b.d.l.	b.d.l.	72.8	26.0	5.34E+04	−6.89	−34.5	−2.16	−0.04	0.47
6a	H. Salaya 4058317, 512871	10/10/2006	45.0	6.83	32.7	−77.5	1.96E+02	1.07	9.31	13.7	0.002	2.05E+02	b.d.l.	b.d.l.	18.5	9.9	1.37E+04	−6.09	−35.7	−3.34	−0.93	0.24
6b	H. Salaya 4058317, 512871	28/09/2009	43.1	6.75	30.1	20	1.99E+02	0.55	7.22	14.4	n.d.	1.86E+02	b.d.l.	1.24	17.2	9.8	1.31E+04	−6.07	−36.5	−3.31	−1.44	0.39
7a	H. Es-Salhine 4063873, 476205	12/10/2006	73.4	6.76	3.53	−290	1.03E+01	0.19	1.02	3.16	0.026	9.79E+00	b.d.l.	0.07	0.60	3.9	9.39E+02	−6.75	−34.9	−5.79	−2.71	−0.02
7b	H. Es-Salhine 4063873, 476205	29/09/2009	72.9	6.74	3.27	−50	9.89E+00	0.14	1.00	3.11	0.012	9.63E+00	b.d.l.	b.d.l.	0.68	3.8	9.14E+02	−7.03	−41.6	−5.82	−2.18	−0.05
8	H. Bourguiba ("populaire") 4069236, 462453	12/10/2006	47.5	6.98	2.94	50	1.21E+01	0.55	1.24	3.68	0.074	7.91E+00	b.d.l.	b.d.l.	0.08	9.3	1.24E+03	−6.73	−34.0	−5.74	−3.63	0.38
9	H. Bourguiba ("basse") 4069316, 462469	12/10/2006	34.0	7.17	1.35	−222	6.17E+00	0.30	1.03	2.10	0.038	2.42E+00	b.d.l.	b.d.l.	0.24	7.6	7.70E+02	−6.80	−35.0	−6.51	−3.3	0.11
10	A. Draham 4068489, 471870	11/10/2006	18.7	4.69	0.3	247	8.94E-01	0.02	0.37	0.30	0.008	1.09E+00	b.d.l.	0.03	0.68	0.1	1.13E+02	n.d	n.d	−7.61	−3.45	−5.02
11	H. Ourahnya 4085870, 491169	12/10/2006	34.8	6.42	2.62	30	1.33E+01	0.51	1.37	5.48	0.002	1.44E+01	b.d.l.	b.d.l.	0.11	5.8	1.32E+03	−6.83	−35.8	−5.43	−3.36	−0.4
12	H. Nefza 4092218, 507232	11/10/2006	33.7	6.51	3.16	−110	9.72E+00	0.18	1.63	10.3	0.039	1.47E+01	0.15	b.d.l.	0.46	8.1	1.51E+03	−5.79	−30.0	−5.57	−2.55	0.06
13a	H. Kef-Ettout 4084390, 509626	11/10/2006	40.8	6.31	10.5	−110	5.29E+01	0.85	3.29	21.0	0.150	7.13E+01	b.d.l.	4.54	0.12	7.1	4.96E+03	−6.09	−33.1	−4.24	−3.16	0.03
13b	H. Kef-Ettout 4084390, 509626	29/09/2009	39.0	n.d	8.3	n.d	n.d	n.d	n.d	n.d	n.d	n.d	n.d	n.d	n.d	n.d	n.d	−6.08	−36.0	n.d	n.d	n.d
14	A. El-Hammam (Marwa) 4086086, 536748	28/09/2009	22.4	7.16	0.72	240	1.71E+00	0.09	0.61	5.03	0.016	2.66E+00	b.d.l.	0.09	0.79	4.0	5.33E+02	−6.39	−32.7	−7.01	−1.89	0.02
15a	H. Sidi Abdelkader 4110174, 561458	09/10/2006	42.3	6.27	25.7	−112	1.38E+02	2.04	18.5	53.9	0.002	1.54E+02	b.d.l.	0.72	48.3	5.9	1.27E+04	−4.23	−21.8	−3.58	−0.51	0.14
15b	H. Sidi Abdelkader 4110174, 561458	27/09/2009	43.6	6.22	19.5	n.d	n.d	n.d	n.d	n.d	n.d	n.d	n.d	n.d	n.d	n.d	n.d	−4.29	−23.2	n.d	n.d	n.d
16	H. Sidi Ben Abbès 4110189, 561473	27/09/2009	42.0	6.30	27.2	33	1.39E+02	1.35	18.3	55.9	0.000	1.61E+02	0.11	b.d.l.	46.2	5.8	1.29E+04	−4.11	−15.6	−3.56	−0.04	0.07
17	H. Echfa (Ichkeul) 4110204, 561443	27/09/2009	42.1	6.23	20.8	n.d	n.d	n.d	n.d	n.d	n.d	n.d	b.d.l.	b.d.l.	n.d	n.d	n.d	−4.27	−23.1	n.d	n.d	n.d
18a	A. El-Hammam (Utique) 4102028, 594523	09/10/2006	38.6	7.21	2.73	−60	1.39E+01	0.33	3.02	3.38	0.039	1.24E+01	b.d.l.	0.23	1.73	8.1	1.47E+03	−5.67	−31.4	−5.49	−2.42	0.36
18b	A. El-Hammam (Utique) 4102028, 594523	27/09/2009	35.6	7.50	3.6	52	2.02E+01	0.28	3.62	4.84	0.028	2.02E+01	0.03	0.05	2.46	6.1	1.83E+03	−5.59	−31.5	−5.15	−1.68	0.55
22	A. Jebel Oust 4043919, 595741	03/10/2009	53.1	6.34	43.3	n.d	2.23E+02	3.74	17.3	51.8	n.d.	2.19E+02	b.d.l.	b.d.l.	55.7	9.2	1.75E+04	−6.07	−44.8	−3.73	−0.75	0.61

27	F. Sahnoun (Jannet) 3944800, 560863	17/10/2006	23.2	7.54	0.54	45	1.11E+00	0.09	1.58	2.29	0.030	7.20E-01	0.01	0.07	0.62	3.7	3.81E+02	−6.40	−39.1	−7.73	−2.79	0.1
29	A. Maamar (H. Sollah) 3918256, 556021	17/10/2006	34.9	6.26	59.3	−353	3.13E+02	8.33	27.3	67.3	0.002	4.33E+02	2.00	b.d.l.	32.4	7.5	2.68E+04	−6.62	−45.0	−2.79	−22.11	−0.42
30	A. Chenama (A. Mouailha) 3916942, 549495	30/09/2009	29.1	6.32	25.7	−225	1.85E+02	3.16	15.5	43.7	n.d.	2.09E+02	0.14	b.d.l.	29.3	6.6	1.47E+04	−7.45	−38.9	−3.29	−6.4	−0.5
31	A. Mizeb (Safia) 3973336, 489036	30/09/2009	16.1	7.44	0.43	95	5.48E-01	0.02	1.08	3.73	0.021	5.90E-01	b.d.l.	0.31	0.54	4.0	4.09E+02	−7.84	−49.1	−8.13	−2.13	0.1
32	A. Thala 3935399, 470659	13/10/2006	20.0	7.45	0.89	77	1.07E+00	0.07	2.53	4.97	0.051	1.30E+00	b.d.l.	0.89	1.94	4.6	6.35E+02	−6.65	−45.4	−7.51	−2.06	0.34
33	F. Sidi Boulaaba 3900858, 477238	13/10/2006	47.2	6.84	4.08	−155	1.22E+01	0.43	5.34	10.8	0.054	8.14E+00	0.03	b.d.l.	16.6	3.4	1.88E+03	−8.26	−56.7	−5.75	−1.05	0.18
34	F. Sidi Ahmed Zarouk Z1 3810949, 476376	13/10/2006	29.1	6.51	20.4	−275	2.06E+02	4.06	16.1	36.3	0.002	2.13E+02	1.31	b.d.l.	39.0	6.8	1.58E+04	−7.14	−49.8	−3.25	−12.17	−0.09
35	F. Sidi Ahmed Zarouk Z3 3811485, 476264	13/10/2006	28.7	6.65	21.3	114	1.52E+02	3.29	14.9	32.3	0.002	1.59E+02	0.99	0.81	38.8	6.2	1.24E+04	−7.29	−48.8	−3.49	−0.76	0.15
Eastern samples																						
19	A. El-Ariane 4065274, 619429	08/10/2006	47.7	6.07	32.8	206	1.70E+02	3.70	12.7	50.2	0.241	2.00E+02	b.d.l.	b.d.l.	25.3	9.9	1.42E+04	−5.66	−33.0	−3.39	−0.83	0.19
20	A. Echfa (Korbous) 4075691, 639811	09/10/2006	52.7	6.57	26.7	90	1.10E+02	2.10	14.4	39.4	0.002	1.34E+02	0.54	b.d.l.	30.8	7.9	1.03E+04	−5.01	−26.2	n.d	n.d	n.d
21	A. El-Atrous (Korbous) 4076906, 639935	08/10/2006	58.0	6.30	29.6	−200	1.11E+02	1.89	13.8	38.9	0.002	1.37E+02	0.99	b.d.l.	33.2	5.3	1.04E+04	−4.99	−26.9	−3.72	−0.86	0.2
23	H. Jedidi 4028517, 624445	18/10/2006	53.3	6.66	4.49	35	2.32E+02	4.19	8.17	34.0	0.002	2.38E+02	b.d.l.	b.d.l.	33.9	7.0	1.68E+04	−6.04	−39.0	−3.2	−0.87	0.52
24	H. Zriba 4022550, 607773	19/10/2006	44.1	6.57	13.1	154	4.22E+01	0.95	11.3	33.2	0.208	4.97E+01	b.d.l.	b.d.l.	40.9	4.1	5.79E+03	−5.66	−36.1	−4.51	−0.52	0.25
25	A. Garci 4000811, 613123	17/10/2006	23.1	6.63	3.22	30	1.55E+01	0.42	4.64	7.17	0.102	9.96E+00	b.d.l.	0.12	2.94	16.8	2.10E+03	−5.48	−36.7	−5.53	−1.97	0.14
26	F. Sidi Abdelhamid 3962682, 649531	03/10/2009	22.2	7.39	12.1	−205	1.04E+02	0.59	12.4	12.9	n.d.	1.06E+02	b.d.l.	0.25	24.6	3.0	7.97E+03	−5.59	−37.1	−3.78	−0.68	0.11
28	F. Oued Kharrouba (Sabrine) 3942387, 583388	30/09/2009	25.3	7.64	0.54	40	2.09E+00	0.50	0.94	1.96	0.081	9.51E-01	b.d.l.	0.22	0.55	3.8	4.26E+02	−5.27	−30.2	−7.36	−2.38	0.14
41	F. Zarat 3724907, 623871	15/10/2006	31.5	7.27	4.48	−27	1.39E+01	0.39	8.49	13.2	0.124	1.33E+01	0.06	0.37	19.2	2.5	2.28E+03	−6.95	−47.5	−5.48	−0.98	0.31
42	F. Alaya 3722884, 622751	15/10/2006	31.6	7.14	4.28	69	1.41E+01	0.36	8.60	13.5	0.122	1.37E+01	0.06	0.39	19.5	2.5	2.32E+03	−6.99	−47.1	−5.46	−0.97	0.19
43	F. Les Sirènes 3748188, 683623	16/10/2006	30.4	7.42	12.5	−180	7.39E+01	0.95	11.3	14.4	0.002	6.89E+01	0.57	b.d.l.	28.8	2.6	6.19E+03	−6.33	−44.0	−4.11	−1	0.34
Saharan samples																						
36	H. Mahassen 3763954, 429972	14/10/2006	63.0	7.07	6.08	−190	1.22E+01	2.00	2.83	15.26	0.002	1.20E+01	b.d.l.	b.d.l.	19.33	2.7	2.22E+03	−7.50	−53.4	−5.61	−0.83	0.63
37	H. Ras El-Aïn 3729020, 498612	14/10/2006	49.3	8.00	5.72	−20	1.55E+01	0.82	4.68	11.62	0.002	1.71E+01	0.12	b.d.l.	14.95	2.1	2.14E+03	−8.14	−60.2	−5.34	−1.09	1.12
38	F. Ras El-Aïn 3729020, 498612	15/10/2006	64.0	7.28	6.77	−243	1.32E+01	0.95	4.91	11.78	0.002	1.67E+01	0.10	b.d.l.	14.50	2.2	2.07E+03	−8.48	−61.6	−5.43	−1.08	0.65
39	F. El-Hamma F2 3753067, 562663	15/10/2006	67.3	6.73	7.22	−204	1.37E+01	1.10	5.20	17.25	0.002	1.75E+01	b.d.l.	0.06	19.08	2.5	2.46E+03	−8.35	−61.4	−5.41	−0.85	0.35
40	F. El-Hamma F9 3753067, 562663	15/10/2006	63.6	6.81	8.52	−197	2.01E+01	1.00	5.45	19.18	0.002	2.27E+01	0.16	b.d.l.	19.88	2.0	2.85E+03	−8.28	−59.6	−5.14	−0.84	0.3

A stands for *Aïn*, the arab word for spring, F for drilled wells, and H for hammam.
Location (North and East) of sampling points refers to the UTM system (WGS84).
Conductivity is in mS/cm at 20 °C. $\delta^{18}O$ and δD values are in ‰ vs. V-SMOW. Total alkalinity(Alk.) is expressed in meq·L^{-1} of HCO_3. Saturation Indexes (SI) of the main soluble mineral phase in Tunisia geological formations are also listed (calculated with the PHREEQC code, Parkhurst and Appelo, 1999).
n.d. = not determined; b.d. = below detection limit.

Table 2
Dissolved gas and carbon and helium isotopes composition of Tunisian groundwaters.

Sample	Site name	P_{tot}	N_2	O_2	CO_2	H_2	CO	CH_4	TDIC	$\delta^{13}C_{TDIC}$	$\delta^{13}C_{CO2}$	^4He	^4He	$^4He/^{20}Ne$	$^4He/^{20}Ne$	R/R_a	R/R_a	^4He	^4He	R/R_a	R/R_a
		atm.	% vol	% vol	% vol	% vol	% vol	% vol	mol/l	‰	‰	mes (1)	mes (2)	mes (1)	mes (2)	mes (1)	mes (2)	xs (1)	xs (2)	xs (1)	xs (2)
Atlasic samples																					
1	H. Mallègue	2.38	85.80	9.59	4.60	2.7E-03	8.2E-04	7.4E-03	1.1E-02	−2.61	−7.02	67.5	n.d	6.937	n.d	0.09	n.d	65	n.d	0.055	n.d
2	H. Bezzaz	n.d	n.d	n.d	n.d	n.d	n.d	n.d	n.d	n.d	n.d	8.04	8.71	0.975	1.071	0.42	0.395	5.88	6.58	0.213	0.204
3	H. Ouchtata	1.08	82.98	0.06	9.98	b.d.l.	4.1E-05	7.0E + 00	1.4E-02	−0.56	−5.19	35.2	n.d	2.146	n.d	0.137	n.d	30.9	n.d	0.019	n.d
4	H. Ali Daoua	1.34	80.92	3.70	15.36	2.8E-03	3.1E-04	1.8E-02	1.6E-02	−0.41	−4.30	28.5	29.8	2.929	3.307	0.179	0.174	26	27.4	0.1	0.104
5a	H. Biadha	1.28	59.68	0.07	40.24	5.2E-03	1.7E-04	9.6E-04	3.9E-02	2.89	−0.93	2.73	2.88	1.167	3.789	0.424	0.247	2.12	2.68	0.262	0.191
5b	H. Biadha	n.d	n.d	n.d	n.d	n.d	n.d	n.d	n.d	n.d	n.d	2.5	2.5	4.310	1.678	0.229	0.349	2.35	2.11	0.179	0.231
6a	H. Salaya	1.68	85.47	9.43	5.08	3.1E-03	b.d.l.	2.7E-04	1.2E-02	−0.48	−5.05	173.9	n.d	13.336	n.d	0.121	n.d	170	n.d	0.104	n.d
6b	H. Salaya	1.11	90.68	0.11	9.19	b.d.l.	2.1E-04	1.1E-02	1.2E-02	−6.26	−10.78	107	119	7.698	7.933	0.135	0.134	103	115	0.105	0.105
7a	H. Es-Salhine	3.01	95.62	1.60	2.77	8.9E-04	6.6E-05	1.9E-03	5.1E-03	−5.67	−7.29	13.7	n.d	1.745	n.d	0.368	n.d	11.6	n.d	0.26	n.d
7b	H. Es-Salhine	0.91	72.44	0.37	13.86	n.d	b.d.l.	1.3E + 01	5.6E-03	−10.09	−11.45	15.7	16.4	2.096	2.207	0.35	0.335	13.7	14.5	0.259	0.248
8	H. Bourguiba (“populaire”)	2.10	93.00	2.47	4.52	1.2E-03	3.2E-04	3.1E-03	1.1E-02	−3.10	−7.32	n.d	n.d	n.d	n.d	n.d	n.d	n.d	n.d	n.d	n.d
9	H. Bourguiba (“basse”)	1.45	94.52	1.77	3.69	1.2E-03	b.d.l.	1.3E-02	9.1E-03	−4.54	−10.13	62.9	58	3.709	3.418	0.204	0.2	58.5	53.6	0.144	0.135
10	A. Draham	n.d	n.d	n.d	n.d	n.d	n.d	n.d	n.d	n.d	n.d	n.d	n.d	n.d	n.d	n.d	n.d	n.d	n.d	n.d	n.d
11	H. Ourahnya	n.d	n.d	n.d	n.d	n.d	n.d	n.d	n.d	n.d	n.d	36.8	37.9	2.564	2.411	0.147	0.152	33	33.8	0.052	0.05
12	H. Nefza	1.93	86.83	7.07	6.10	2.5E-03	5.1E-05	1.8E-04	1.1E-02	−4.52	−9.14	51.6	n.d	2.571	n.d	0.209	n.d	46.3	n.d	0.121	n.d
13a	H. Kef-Ettout	1.70	92.51	0.11	7.38	1.6E-03	0.0E + 00	5.8E-04	1.0E-02	−3.48	−7.45	43.9	77.5	2.698	3.827	0.116	0.123	39.6	72.2	0.023	0.06
13b	H. Kef-Ettout	n.d	n.d	n.d	n.d	n.d	n.d	n.d	n.d	n.d	n.d	17.4	n.d	1.289	n.d	0.227	n.d	13.8	n.d	0.033	n.d
14	A. El-Hammam (Marwa)	1.61	83.59	15.34	1.06	b.d.l.	4.1E-03	3.6E-04	4.6E-03	−10.20	−17.15	18.9	18.2	0.325	0.329	0.872	0.858	3.64	3.74	0.399	0.367
15a	H. Sidi Abdelkader	1.42	89.38	2.96	7.66	b.d.l.	b.d.l.	1.0E-03	8.4E-03	−2.44	−6.28	37.4	59.1	0.822	5.175	0.651	0.427	25.5	56.1	0.495	0.397
15b	H. Sidi Abdelkader	n.d	n.d	n.d	n.d	n.d	n.d	n.d	n.d	n.d	n.d	113	n.d	8.188	n.d	0.417	n.d	110	n.d	0.399	n.d
16	H. Sidi Ben Abbès	1.15	86.91	0.07	12.99	b.d.l.	b.d.l.	2.1E-02	9.3E-03	−9.67	−12.99	100	112	0.877	7.619	0.603	0.425	70.2	108	0.441	0.405
17	H. Echfa (Ichkeul)	n.d	n.d	n.d	n.d	n.d	n.d	n.d	n.d	n.d	n.d	86.4	108	7.927	7.714	0.416	0.428	83.5	105	0.397	0.408
18a	A. El-Hammam (Utique)	1.26	85.38	13.37	1.25	2.1E-03	b.d.l.	2.0E-04	8.5E-03	−7.75	−13.78	7.57	9.07	2.273	2.296	0.547	0.558	3.71	4.42	0.093	0.107
18b	A. El-Hammam (Utique)	1.11	91.69	5.80	2.51	b.d.l.	7.1E-05	1.2E-04	6.8E-03	−11.23	−17.10	10.1	10	0.526	0.549	0.52	0.524	5.06	5.22	0.058	0.098
22	A. Jebel Oust	1.66	80.59	8.89	10.50	b.d.l.	1.3E-04	1.1E-03	1.3E-02	−3.88	−7.06	107	113	8.492	7.847	0.228	0.223	103	109	0.203	0.197
27	F. Sahnoun (Jannet)	1.05	97.01	2.16	0.84	b.d.l.	6.4E-05	5.2E-04	n.d	n.d	n.d	11.4	11.2	0.535	0.521	0.521	0.52	5.82	5.57	0.076	0.049

29	A. Maamar (H. Sollah)	1.20	83.97	1.65	13.26	b.d.l.	b.d.l.	8.8E-01	1.2E-02	−8.81	−12.72	2339.4	2759.6	73.381	73.121	0.021	0.021	2330	2750	0.018	0.018
30	A. Chenama (A. Mouailha)	n.d	n.d	n.d	n.d	n.d	n.d	n.d	n.d	n.d	n.d	3260	4070	60.708	80.276	0.025	0.026	3250	4050	0.021	0.023
31	A. Mizeb (Safia)	0.91	96.04	2.96	1.00	b.d.l.	b.d.l.	1.7E-03	n.d	n.d	n.d	5.12	5.22	0.265	0.288	1.034	1.007	n.d	n.d	n.d	n.d
32	A. Thala	n.d	n.d	n.d	n.d	n.d	n.d	n.d	n.d	n.d	n.d	n.d	n.d	n.d	n.d	n.d	n.d	n.d	n.d	n.d	n.d
33	F. Sidi Boulaaba	2.56	95.41	3.27	1.31	1.4E-03	8.5E-05	7.3E-03	4.1E-03	−5.52	−9.79	159.2	164.3	7.773	7.381	0.054	0.053	154	158	0.022	0.019
34	F. Sidi Ahmed Zarouk Z1	2.22	95.44	0.64	3.62	1.4E-03	2.1E-05	5.3E-02	9.3E-03	−3.88	−9.05	4723	4662	116.187	116.434	0.021	0.021	4713	4652	0.019	0.019
35	F. Sidi Ahmed Zarouk Z3	1.65	93.40	3.08	3.40	6.5E-03	2.5E-04	1.6E-04	7.9E-03	−4.31	−9.91	1777	1452	75.778	69.774	0.023	0.021	1770	1450	0.019	0.018
Eastern samples																					
19	A. El-Ariane	1.92	73.20	6.84	19.92	4.1E-03	3.0E-04	5.7E-03	1.8E-02	−0.30	−2.76	344	527	43.544	35.705	0.287	0.289	34.2	52.3	0.283	0.284
20	A. Echfa (Korbous)	1.09	77.35	6.91	15.73	2.1E-03	b.d.l.	2.0E-03	1.1E-02	−0.38	−3.44	288.8	307.1	22.902	30.466	0.267	0.263	385	304	0.261	0.257
21	A. El-Atrous (Korbous)	2.19	73.25	12.74	13.98	6.9E-03	7.1E-04	7.0E-04	1.1E-02	−0.89	−2.44	441.8	442.7	54.678	54.120	0.266	0.266	440	441	0.263	0.262
23	H. Jedidi	1.72	88.45	5.39	6.09	7.8E-03	4.8E-02	1.7E-02	9.0E-03	0.30	−3.12	20.1	22.9	1.811	1.800	0.712	0.708	17.2	19.6	0.665	0.661
24	H. Zriba	1.04	93.06	1.17	5.76	b.d.l.	1.2E-04	7.1E-03	5.4E-03	−4.56	−8.61	54	33.4	3.902	3.337	0.631	0.621	50.4	30.8	0.605	0.59
25	A. Garci	1.15	78.74	1.81	19.42	b.d.l.	1.3E-04	1.5E-02	2.5E-02	−0.56	−5.70	141	136.9	9.704	8.930	2.392	2.388	137	132.9	2.431	2.431
26	F. Sidi Abdelhamid	1.52	99.19	0.15	0.51	b.d.l.	b.d.l.	6.5E-02	3.3E-03	−5.96	−13.39	3800	n.d	62.500	n.d	0.314	n.d	3790	n.d	0.311	n.d
28	F. Oued Kharrouba (Sabrine)	0.91	98.68	0.08	1.24	b.d.l.	b.d.l.	3.5E-04	4.2E-03	−8.81	−15.88	5.53	5.34	0.287	0.287	1.022	1.04	n.d	n.d	n.d	n.d
41	F. Zarat	1.65	91.85	7.65	0.49	b.d.l.	b.d.l.	2.4E-04	2.7E-03	−5.96	−12.42	23.9	n.d	1.273	n.d	0.239	n.d	19	n.d	0.046	n.d
42	F. Alaya	1.67	94.40	5.13	0.45	b.d.l.	9.7E-05	1.7E-02	2.7E-03	−6.26	−12.75	11.3	16.6	0.556	0.846	0.503	0.335	5.98	11.5	0.074	0.044
43	F. Les Sirènes	1.36	96.16	3.42	0.40	b.d.l.	2.0E-04	1.5E-02	2.8E-03	−10.09	−16.90	651.1	n.d	21.893	n.d	0.121	n.d	643	n.d	0.111	n.d
Saharan samples																					
36	H. Mahassen	3.31	91.82	5.99	1.87	1.5E-03	2.3E-01	9.2E-02	3.7E-03	−7.79	−10.11	115.9	101.8	8.273	7.442	0.042	0.045	112	98.2	0.011	0.011
37	H. Ras El-Aïn	1.48	96.14	3.62	0.21	b.d.l.	1.8E-04	2.3E-02	2.2E-03	−10.83	−15.80	n.d	n.d	n.d	n.d	n.d	n.d	n.d	n.d	n.d	n.d
38	F. Ras El-Aïn	1.46	95.78	2.80	1.42	b.d.l.	b.d.l.	7.2E-04	2.5E-03	−9.67	−12.55	20.2	19.9	1.688	1.605	0.194	0.196	17.1	16.7	0.048	0.042
39	F. El-Hamma F2	2.59	96.88	1.72	1.29	1.4E-03	1.6E-04	1.0E-01	3.0E-03	−10.20	−12.59	404.8	268.2	13.435	12.907	0.036	0.035	397	263	0.017	0.016
40	F. El-Hamma F9	1.66	97.78	0.49	1.59	b.d.l.	b.d.l.	1.3E-01	2.4E-03	−11.23	−13.94	162.1	196.3	6.049	6.541	0.053	0.051	155	188	0.011	0.012

Letters a and b in sample numbers refer to sampling year, 2006 and 2009 respectively. The isotopic composition ($\delta^{13}C_{TDIC}$) is in δ per mil vs. V-PDB. The calculated equilibrium isotopic compositions of gaseous CO_2 ($\delta^{13}C_{CO2}$) are also listed. Measured ($^4He_{mes}$) and neon-corrected ($^4He_{xs}$) helium concentrations are in 10^{-8} cm^3 STP/g (numbers 1 and 2 correspond to the two water samples collected at each site). R/R_ames and R/R_axs are the measured and neon-corrected $^3He/^4He$ ratios scaled to the atmospheric $^3He/^4He$ value (Ra).

uncertainty on measured $^{3}He/^{4}He$ ratios, calibrated against an atmospheric air standard, is better than 0.5%. At each site, two helium samples were collected, which give consistent results (Table 2). Helium concentrations and isotopic ratios were corrected for possible air contamination using the measured $^{20}Ne/^{4}He$ ratios and assuming a pure atmospheric origin for ^{20}Ne (Hilton, 1996).

4. Results

4.1. Chemistry of major ions

The collected water samples are characterized by significant heterogeneity in their chemical–physical features (see Table 1). We identify both cold (T<25 °C) and thermal (T from 25 to 73.4 °C) groundwaters in our dataset. The waters range from dilute (with TDS, as low as 113 mg L^{-1}; Total Dissolved Solid (TDS) content is the calculated sum of the major and minor ion species contents in mg L^{-1}) to saline waters, and show pH values from slightly acidic (e.g. sample 10) to nearly neutral (e.g. samples 27 and 28). Thermal waters are characterized by very high TDS values (up to 53,000 mg L^{-1}), usually even greater than those typical of seawater. Overall, thermal waters display a weak but systematic positive correlation between salinity and pH values, suggesting that their saline burden reflects the temperature-dependent titration of the formerly acidic infiltrating meteoric waters by dissolving host rocks.

The collected water samples belong to all of the four water classification types proposed by Langelier and Ludwig (1942) (Fig. 2). More in the specific, cold waters flowing in the terrains of the Atlasic and Eastern domains have a prevalent bicarbonate earth-alkaline composition characteristic of shallow infiltrated meteoric waters in sedimentary environment. We note however that a few cold water samples, collected near the coast (e.g. sample 26), depart from the bicarbonate-type waters, and trend towards the compositional field of chloride–sulfate alkaline waters; this, when looked in tandem with increasing TDS values, supports some extent of seawater contribution to coastal shallow aquifers, as already reported in Tunisia for instance in the case of the Korba aquifer, Cap Bon (Kouzana et al., 2009, 2010) or the Sfax superficial aquifer (Trabelsi et al., 2005, 2007).

Thermal waters display a large spread of compositions. Samples collected in the Atlasic domain are the most heterogeneous. They have prevalent chloride–sulfate alkaline compositions, with Na as major cation species (Ca prevails only in samples 12 and 33, see Fig. 2); but also spread towards bicarbonate-alkaline compositions (as indicated by the arrow in Fig. 2) to occasionally chloride–sulfate earth alkaline compositions. Thermal groundwaters from the Eastern and Saharan domains, in turn, have more uniform compositions, and cluster in a relatively narrow area along the left segment of Fig. 2.

The contrasted compositional features of Tunisian groundwaters emerge even more evidently when the main anion (Cl, SO_4 and HCO_3) and cation (Na, Ca, and Mg + K) dissolved species are separately analyzed. Inspection of ternary diagrams (Fig. 3a & b) demonstrates that:

(i) Mg and K are a relatively minor species in all Tunisian groundwaters; which, in terms of dissolved cations range from Ca-rich to Na-rich (Fig. 3a). The group of Na-rich waters includes all thermal water samples and most cold groundwaters;

(ii) Bicarbonate is the main anion species in most cold-groundwaters, consistent with the prevailingly meteoric/organic origin of dissolved salts (from atmospheric and soil CO_2) in these poorly mineralized water samples (Fig. 3b). Only in high-TDS cold groundwaters, Cl prevails over HCO_3;

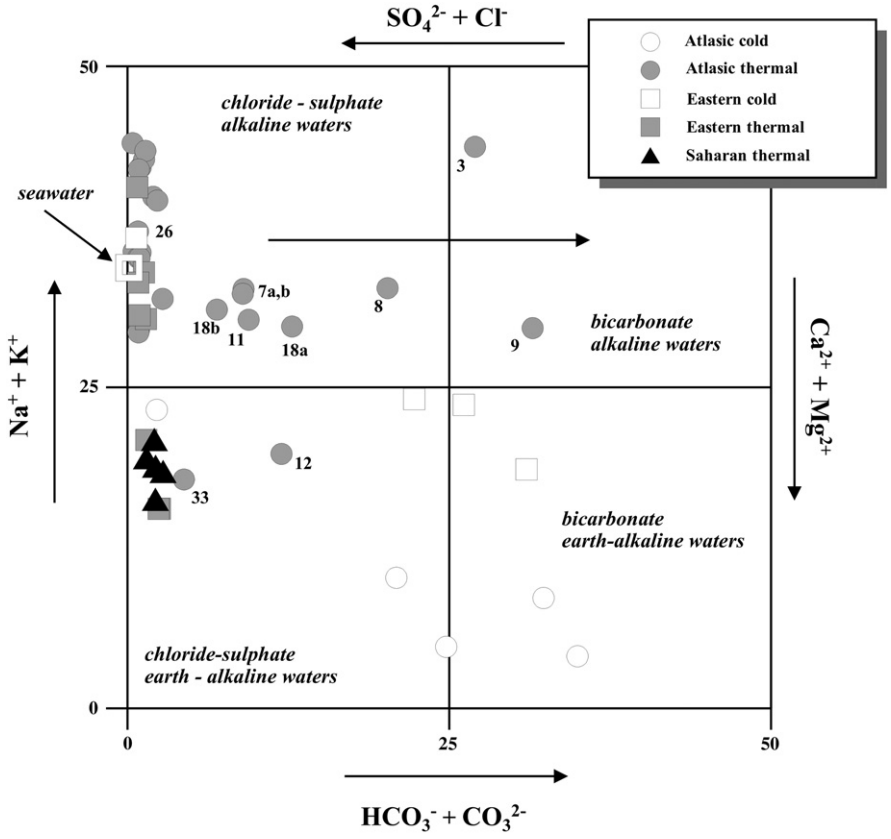

Fig. 2. Langelier–Ludwig classification diagram (Langelier and Ludwig, 1942) of Tunisian groundwaters. The numbers refer to the sampling sites. See text for explanations.

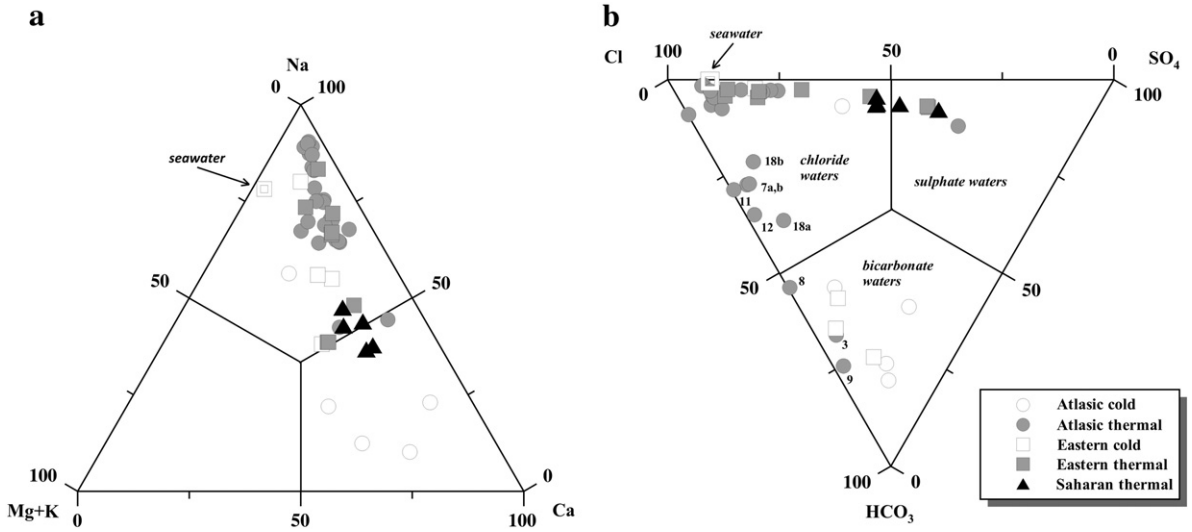

Fig. 3. Ternary plots of major dissolved ions in Tunisian groundwaters (drawn from concentrations in meq/L); (a) cations species and (b) anions species. The wide heterogeneity of both cold and thermal waters composition is clearly supported by the two diagrams.

(iii) Thermal groundwaters from the Atlasic domain are dominantly Cl-type waters, but eventually span from Cl-type to HCO_3-type (Fig. 3b). The shift toward HCO_3-type waters (Fig. 3b) reflects more a lower Cl content (relative to other samples of the Atlasic domain) than a real HCO_3 increase (see Table 1), and is more manifest in a group of thermal groundwaters emerging in the Tellian sector (samples 3, 7a-b, 9, 11, 12, 18a-b);

(iv) Thermal groundwaters from the Eastern and Saharan domains are particularly HCO_3-poor (relative to other anion species); in the triangular diagram of Fig. 3b, these samples define a fairly narrow (and almost continuous) compositional trend from Cl-type waters (Eastern domain) to SO_4-type waters (Saharan Domain).

4.2. Water isotopic composition

The results of hydrogen and oxygen isotopic determinations in Tunisian groundwaters, expressed in δ units vs. V-SMOW, are listed in Table 1. The δD and $\delta^{18}O$ values are quite variable, ranging from −61.6 to −15.6‰ and −8.48 to −4.11‰, respectively. The δD–$\delta^{18}O$ scatter diagram (Fig. 4) confirms that all groundwaters are essentially meteoric in origin, with overall limited seawater contribution. The isotopic compositions of groundwaters from Northern (Atlasic + Eastern domains) and Southern (Saharan domain) Tunisia are in stark contrast (Fig. 4). The former have isotopic compositions falling within the field delimited by the Global Meteoric Water Line (GMWL; Craig, 1961) and the Eastern Mediterranean Meteoric Water Line (EMMWL; Gat and Carmi, 1970), and cluster in close proximity of the regional meteoric water lines derived by Celle-Jeanton et al. (2001) from local precipitations in Tunis and Sfax; the latter, on the contrary, plot to the right of the Global Meteoric Water Line and are characterized by δD and $\delta^{18}O$ values far more negative than the range of present-day precipitations. This depleted isotopic signature (with $\delta^{18}O$ and δD values averaging at −8.15‰ and −59.2‰, respectively) is a distinctive feature of the Continental Intercalaire (CI) as shown by Guendouz et al. (1997), indicating that these groundwaters belong to a fossil deep reservoir whose recharge probably occurred early during the late Pleistocene period under different (colder and more humid) climatic conditions (Gonfiantini et al., 1974; Edmunds et al., 2003; Zouari et al., 2003; Trabelsi et al., 2009).

4.3. Gas abundances

Table 2 reports the relative abundances of the major gas species (N_2, O_2, CO_2, CO, CH_4, H_2) in the dry gas phase at equilibrium with each water sample. The ternary plot of Fig. 5 shows that most Tunisian samples have N_2-dominated compositions (from 33 to 99 vol.%; Table 2), supporting a likely atmospheric derivation of the dissolved gasses. Oxygen represents only a relatively small fraction (0.06–15 vol.%; Table 2); indeed, all samples are shifted towards the N_2 corner relative to the representative compositional field of air. The relatively low O_2 contents are not inconsistent with a main atmospheric derivation of the gasses, however : this oxygen depletion (relative to N_2) is probably due to redox reactions between gasses and host rocks (Stumm and Morgan, 1996), and/or consumption of atmospheric oxygen by organic activity at shallow levels.

CO_2 ranges from 0.2 to 40 vol.%. Moderate CO_2-excesses (Fig. 5), relative to atmospheric composition, are observed in several thermal waters from the Atlasic and Eastern domains; suggesting that these groundwater systems are open to contribution from an additional CO_2 source than only atmosphere. The highest CO_2 concentrations, from 20 to 40 vol.% (e.g., samples 5a, 19 and 25 — see Table 2), correspond to CO_2 partial pressures of 0.22, 0.38 and 0.51 atm, respectively, far exceeding those characteristic of the atmosphere (0.00038 atm) and soil (0.01 — 0.001 atm; Brook et al., 1983; Hamada and Tanaka, 2001). On the contrary, samples collected in the Saharan domain are systematically characterized by low CO_2 contents (0.2–3 vol.%).

4.4. Carbon isotope geochemistry

The total dissolved inorganic carbon contents of Tunisian groundwaters (TDIC, given by the sum of CO_{2aq}, HCO_3 and CO_3) are listed in Table 2, together with their isotopic compositions ($\delta^{13}C_{TDIC}$). The TDIC values range from $2\cdot10^{-3}$ to $4\cdot10^{-2}$ mol·L^{-1}, and $\delta^{13}C_{TDIC}$ from −11.23 and +2.89‰ vs. V-PDB (Fig. 6a). This variability of compositions gives a hint for a range of different gas–water interaction environments, and supports a variety of different sources for dissolved carbon (Grassa et al., 2006).

The isotopic composition of TDIC represents an average of the isotopic compositions of the relevant dissolved carbon species, weighted by their respective contents in solution (Zhang et al., 1995). To derive insights into the origin of dissolved carbon in Tunisia

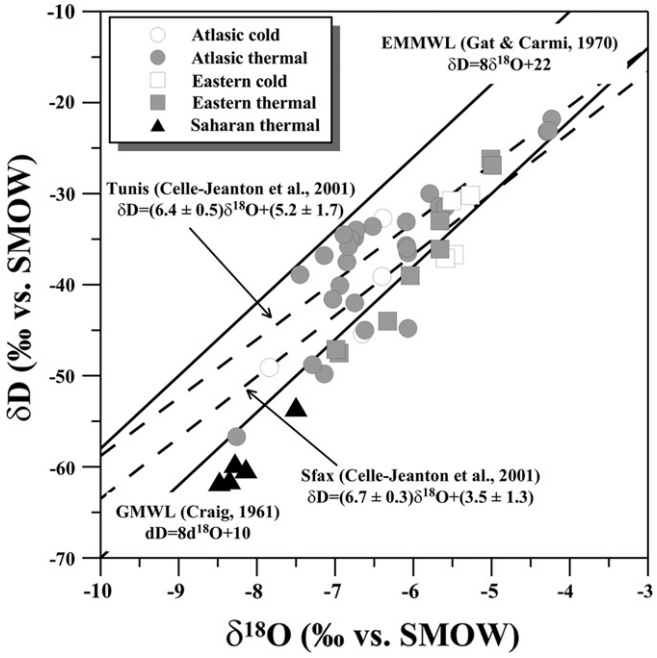

Fig. 4. δD vs. $\delta^{18}O$ diagram of Tunisian groundwaters. The solid lines correspond to the Global Meteoric Water Line (GMWL; Craig, 1961) and the Eastern Mediterranean Meteoric Water Line (EMMWL; Gat and Carmi, 1970); while the dashed lines are indicative of δD and $\delta^{18}O$ isotopic compositions of local rainwaters in Tunis and Sfax (Celle-Jeanton et al., 2001).

groundwaters, the isotopic compositions of gaseous CO_2 at isotopic equilibrium with each water sample (at the given T, pH and TDIC) have been calculated by Eq. (1). This relation takes into account the dependence of equilibrium fractionations between gaseous CO_2 and the different dissolved carbon species ($CO_{2(aq)}$, $HCO_{3(aq)}^{-}$ and $CO_{3(aq)}^{2-}$). The extent of these TDIC-CO_2(g) fractionations thus depends on T and pH of the solutions, and from the enrichment factor (ε) of each species with respect to gaseous CO_2 (Zhang et al., 1995).

$$\delta^{13}C_{CO2g} = \delta^{13}C_{TDIC} - \left(\varepsilon_{CO2aq-CO2g} \times \chi_{CO2aq}\right) - \left(\varepsilon_{HCO3-CO2g} \times \chi_{HCO3}\right) - \left(\varepsilon_{CO3-CO2g} \times \chi_{CO3}\right) \quad (1)$$

where the different enrichment factor values (ε) are taken from Deines et al. (1974) and χ_{CO2aq}, χ_{H2CO3} and χ_{CO3} are the equilibrium molar ratios of aqueous carbon species at the same conditions.

The so-obtained $\delta^{13}C_{CO2}$ values (Table 2) range from −17.15 to −0.93‰ vs. V-PDB, and are plotted in Fig. 6b against the corresponding CO_2 content. Fig. 6b shows that CO_2 isotopic compositions become more positive upon increasing CO_2 content. Samples from the Saharan domain, being the most CO_2-poor (see also Fig. 5), are also characterized by the most ^{13}C-depleted isotopic compositions ($\delta^{13}C_{CO2} < -9$‰ vs. V-PDB), and approach the typical compositions of organically-derived CO_2 ($\delta^{13}C_{CO2,bio} < -18$‰ vs. V-PDB). We stress, however, the lack of very negative (<−18‰ vs. V-PDB) samples in our dataset, which we ascribe to both the "buffering" action played by calcite dissolution (see Section 5.2), and to the fact that soil cover is relatively poorly developed in arid regions like Tunisia (thus reducing biologic CO_2 production in the soil environment). Intermediate C isotopic compositions are observed for a large cluster of samples which, in spite of their relatively minor CO_2 content ($\chi_{CO2} < 0.1$ mol·mol^{-1}), spread in $\delta^{13}C_{CO2}$ from −10 to −5‰ vs. V-PDB. Finally, the less negative isotopic compositions ($\delta^{13}C_{CO2}$ of −4 to −1‰ vs. V-PDB) correspond to the most CO_2-rich samples from the Atlasic and Eastern domains.

Fig. 6b compares our derived CO_2 isotopic compositions of Tunisian groundwaters with analogous data from volcanic (Pantelleria Island) and non-volcanic districts of nearby Sicily. This shows that Tunisian groundwaters have $\delta^{13}C_{CO2}$ compositions overlapping the measured compositional range of thermal waters from central-western Sicily, an area of remarkably similar geodynamic context (Grassa et al., 2006); while they are strongly dissimilar in composition (more ^{13}C-rich) to CO_2 in thermal waters from Pantelleria (Parello et al., 2000), in the Sicily channel rift (Fig. 1).

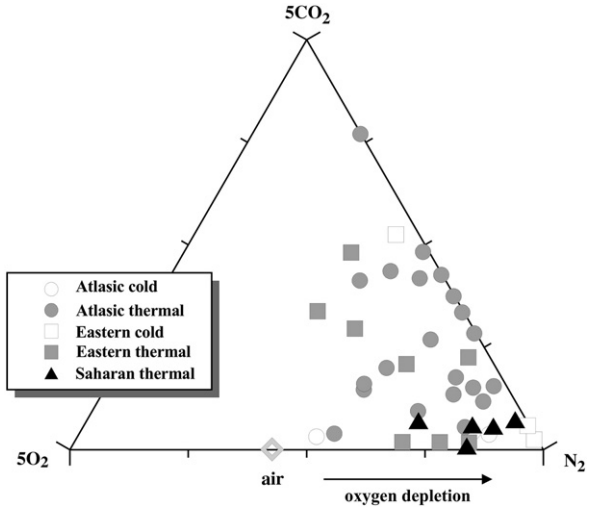

Fig. 5. Ternary plot of the main species (N_2, CO_2 and O_2) in gas phase at equilibrium with each groundwater sample, drawn from the volumetric percentage (vol.%) reported in Table 2. Tunisian groundwaters display N_2-dominated compositions, and are characterized by oxygen depletion relative to air composition (likely due to redox reactions in the hydro-cycle). They also manifest CO_2-enrichment (relative to air), pointing to the existence of additional CO_2 sources.

4.5. Helium isotopes

Helium isotopes results are given in Table 2. All $(^3He/^4He)_{xs}$ values, where $(^3He/^4He)_{xs}$ is the isotopic ratio of non-atmospheric helium deduced from the neon correction, are below the atmospheric ratio (Ra) except for sample 25 (Ain Garci site) which reaches 2.4 Ra (Fig. 7). When gas and water were sampled simultaneously, we observe a good agreement between both isotopic ratios (Table 3).

The lowest $^3He/^4He$ values, comparable to the crustal production ratio of 0.01–0.05 Ra (Ballentine and Burnard, 2002), are found in the central and southern parts of the country (Figs. 7 and 8), associated with the Atlasic domain and the Saharan Platform, respectively. In the Tellian sector (northwestern Tunisia), the $^3He/^4He$ values are still quite low (0.13 ± 0.08 Ra) but clearly above the crustal ratio. West of the Tellian sector, the Marwa site (sample 14) and the Ichkeul group (samples 15-16-17) display higher $^3He/^4He$ values, around 0.4 Ra (Figs. 7 and 8). In the Eastern Domain, $^3He/^4He$ values range from 0.25 to 0.65 Ra and up to 2.4 Ra in Ain Garci (sample 25), a CO_2 rich mineral spring located some 30 km south of the city of Zaghouan. For this water, the low tritium (1.2 ± 0.1 TU – Fourré et al., in prep.) and high helium (135×10^{-8} cm^3 STP/g) contents rule out any significant tritiogenic ^3He contribution to the elevated $^3He/^4He$ ratio.

Measured helium concentrations are well above the air-saturated value ($4–5 \times 10^{-8}$ cm^{3}STP/g), ranging from 7.6 to 4723×10^{-8} cm^{3}STP/g (Table 2), except for sample 5 (Hammam Biadha) where values measured in 2006 and again in 2009 are below the atmospheric solubility

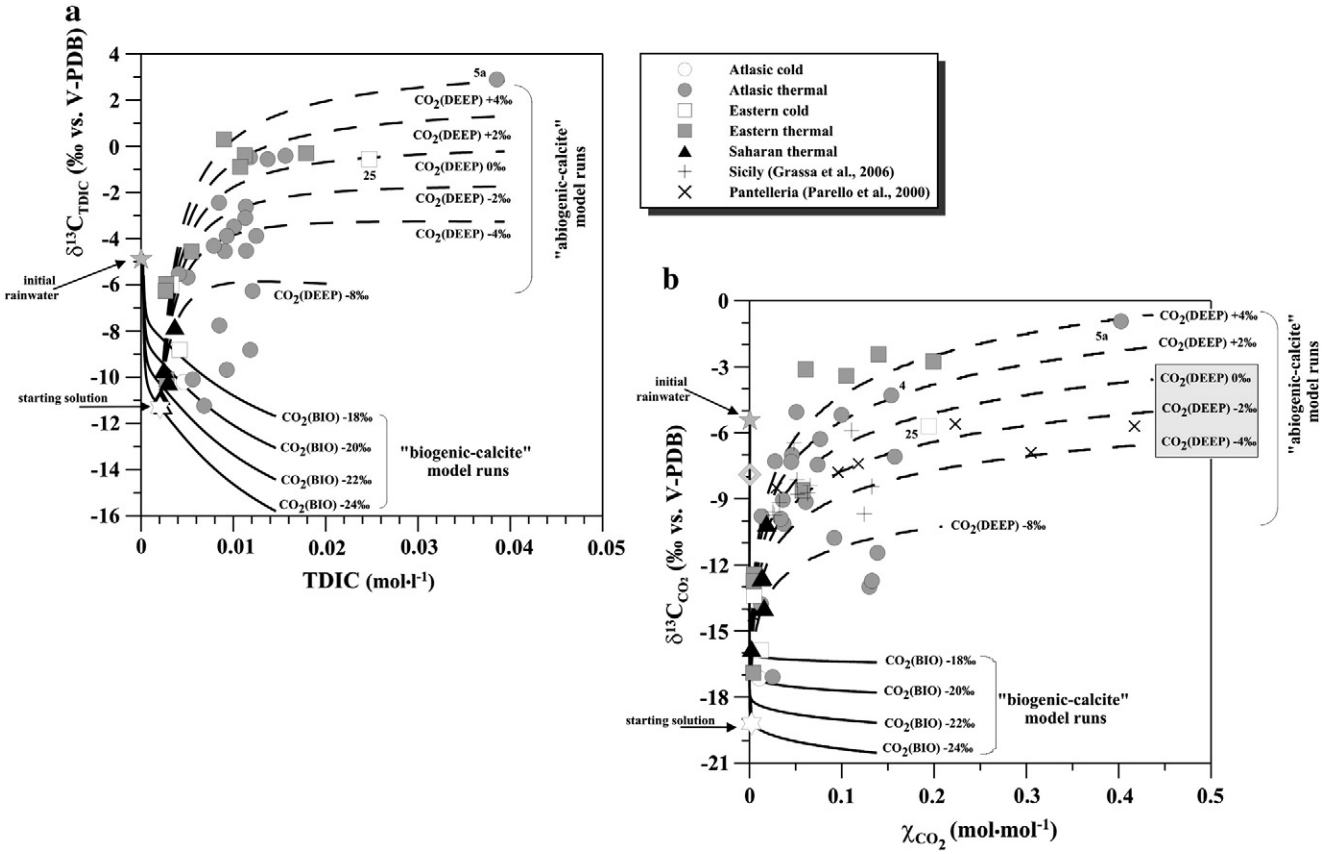

Fig. 6. (a) Measured TDIC contents of Tunisian groundwaters, plotted vs. the corresponding $\delta^{13}C_{TDIC}$ values. Measured compositions are compared with the results of model runs (shown by curves), which simulate the theoretical variations of dissolved carbon and $\delta^{13}C_{TDIC}$ when biogenic (dashed lines) and abiogenic (solid lines) CO_2 are added (in consecutive steps) to the starting solution (equilibrium with calcite was forced at each step of the simulations). Curves were drawn following Chiodini et al. (2000), and are relevant to CO_2-water-calcite equilibrium in a carbonate groundwater system. See text for explanation. (b) Binary plot contrasting the CO_2 contents of Tunisia groundwaters with the respective C-isotopic compositions. We use the modeled $\delta^{13}C_{CO2}$ compositions (from Eq. (1)) – in addition to measured $\delta^{13}C_{TDIC}$ values – since the former are better suited (than measured values) to derive insights into the origin of dissolved carbon in Tunisia groundwaters (allowing direct comparison with isotopic signature of the main C reservoirs), and because they make comparison with literature data more straightforward. In the x-axis of (b), we report the CO_2 molar fractions (χCO_2) in the gas phase at equilibrium with each water sample at the sampling T (from data reported in Table 2); while in the y-axis we report the relative $\delta^{13}C_{CO2}$ values (calculated from $\delta^{13}C_{TDIC}$ values using a re-arranged relation (1); Zhang et al., 1995). Solid and dashed lines are the results of model simulations (as in Fig. 6a). In the same figure, compositional data from a number of thermal manifestations from Pantelleria Island (Parello et al., 2000) and Western-Central Sicily (Grassa et al., 2006), are also shown for comparison. The gray shaded area corresponds to the isotopic range of magmatic carbon in Italy.

value, probably due to helium stripping by the strong CO_2 bubbling which occurs at this site. Particularly high values, in the range 1777–4723×10^{-8} cm^3STP/g (samples 26, 29, 30, 34, 35) are observed on a SW–NE transect across central Tunisia going from Gafsa to Sousse (Fig. 8), associated with well documented tectonic features (see discussion below).

4.6. He-CO_2 characteristics

Fig. 9 displays the CO_2–helium results plotted on a CO_2–^{4}He–^{3}He diagram (after Giggenbach et al., 1993). The $CO_2/^3$He ratios range from 2.6×10^6 to 3.5×10^{11}. In contrast with typical volcanic environments where helium and CO_2 relationship results in rather well defined $CO_2/^3$He values (Hilton et al., 2002), the Tunisian data set shows five orders of magnitude variability, going from lower than MORB values ($CO_2/^3He=2\times10^9$) to crustal values ($CO_2/^3He>10^{10}$), with most values however characterized by $CO_2/^3$He ratios between the typical MORB ($CO_2/^3He=2\times10^9$) and global average arc values ($CO_2/^3He=1.2\times10^{10}$). This wide variability is best explained, as discussed below (see Section 5.2), by the fact that the respective origin of CO_2 and helium isotopes are largely decoupled in the system, with most samples characterized by crustal helium and metamorphic CO_2 mixed in variable amounts.

5. Discussion

5.1. Geochemical processes : sources of salts and link with geology

From a chemical viewpoint, the most striking feature of Tunisian thermal waters is their large heterogeneity (see Figs. 2 and 3). This is indeed not surprising in light of the variability of geological landforms, terrains, and structural settings in the various parts of the country. In most geothermal fluids hosted by active volcanic systems (Goff and Janik, 2000), the sources of dissolved chemicals include (i) the interaction of deep-rising magmatic gasses (sourcing the majority of Cl, S and C) with infiltrating surface waters (formerly meteoric or marine in origin), and (ii) the resultant high-temperature gas–water–silicate hydrolysis reactions, which supply cation species to hydrothermal solutions. In these hydrothermal systems, the contrasting chemical compositions of the various surface manifestations generally arise from the fact that they correspond to different steps in the maturation path of infiltrating waters (Giggenbach, 1988). In sedimentary environments such as Tunisia, however, the sources of chemicals in thermal waters are more challenging to interpret, because the mineralogical and chemical properties of the hosting aquifers are inherently more heterogeneous, and because physical (e.g., heat flux, stress regime) and hydrological conditions (e.g., infiltration depth and residence time in reservoir) are likely to be

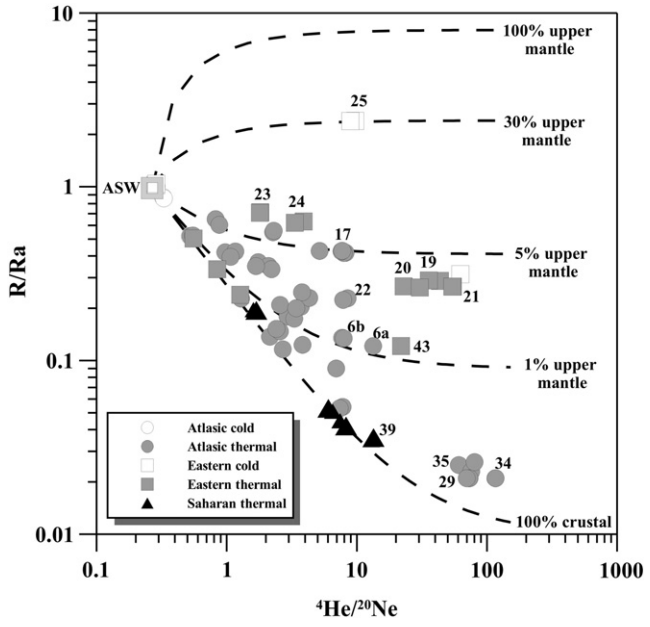

Fig. 7. Helium isotopes results plotted as R/Ra vs. $^4He/^{20}Ne$. The dotted lines depict mixing trends between the atmospheric and the crustal components, with various addition of an upper mantle component with $R = 8 \times Ra$.

different and specific to each manifestation. In view of this complexity, and taking into account that our regional-scale geochemical prospecting precludes detailed investigation of each single manifestation, we attempt below at discussing the key control factors/processes in the evolution of Tunisian thermal waters.

First, we observe that most thermal waters from the Atlasic and Eastern domains have a prevalent NaCl composition (Figs. 2 and 3). Accepting the fact that groundwater–seawater interactions are modest (Fig. 4) if not locally near the coast, and that contribution from high-T Cl-bearing magmatic gasses is negligible (as indicated by the low $^3He/^4He$ ratios), we argue then that the interaction of infiltrating waters with halite-bearing Triassic evaporites is the most likely source of both Na and Cl. There is a fair positive correlation between sodium and chlorine contents (Fig. 10a), and Cl-rich waters ($Cl/\sum anions > 0.7$; see Table 1) belonging to the Atlasic and Eastern domains are all characterized by molar Na/Cl ratios of ~1 (the stochiometric Na/Cl ratio of halite dissolution; Fig. 10a). These groundwaters have Saturation Indexes (SI) for halite (SI_{Halite}) from −6 to −2 (Table 1), suggesting they have extensively leached soluble salts, though not having reached equilibrium with halite, yet.

Secondly, we identify a typical SO_4-type composition for the thermal waters from the Saharan domain. Most of these waters were collected from deep artesian wells tapping the CI, and thus consistently have the typical Na, Ca–SO_4 composition (see Fig. 3), as already revealed by earlier studies (Edmunds et al., 2003). Clearly, this composition highlights that dissolution of gypsum and/or anhydrite, which are minor but recurring constituents of the CI sandstone formations, plays a major role in groundwater mineralization. It is not surprising to observe then, that all thermal waters from the Saharan domain cluster along the gypsum/anhydrite dissolution line (at equivalent Ca to SO_4 ratios of 1:1: see Fig. 10b), and are close to equilibrium with gypsum (SI_{gypsum} of −0.6 to −0.4; Table 1). The same Fig. 10b reveals that several thermal waters from the Atlasic and Eastern domains also plot along the same gypsum/anhydrite dissolution line. This suggests that dissolution of sulfate minerals, likely hosted in the Triassic evaporitic sequence and/or in the upper Cretaceous series (Fig. 1), contributes to water chemistry also in these parts of the country.

Thirdly, carbonate formations are widespread all over Tunisia (included in the Triassic evaporitic sequence and in the Cretaceous to Cenozoic limestones). Yet, carbonate mineral dissolution visibly affects water chemistry only where more-easily leachable evaporitic minerals are absent (or limited). It is noteworthy to observe, in fact, that while a relatively narrow band of Triassic evaporites forms the NE–SW-trending "diapir zone" extending from Bizerte to Le Kef (see black-colored band in Fig. 1), no major Triassic outcrop is reported in the Tellian sector (northernmost part of the Atlasic domain; Fig. 1), where Oligo-Miocene Numidian Flysch units mainly crop out : thermal waters collected in this part of the country (samples 3, 7a-b, 9, 11, 12, 18a-b; see Fig. 1) consistently depart from the gypsum/anhydrite dissolution line (Fig. 10b), implying that evaporitic mineral dissolution is an unquestionably more marginal process : they have dominant Na, Ca-HCO_3 compositions (Fig. 3), and display Ca/HCO_3 ratios of ~1 (see cluster of data points falling within the white area in Fig. 10c), typical of waters undergoing calcite dissolution as the prevalent mineralization process. These water samples consistently are at equilibrium conditions with calcite ($-0.4 < SI < 0.6$).

The key source processes controlling the chemistry of Tunisian thermal groundwaters are summarized in Fig. 10d. This confirms that Na and Cl concentrations are primarily controlled by dissolution of the saliferous Triassic formations rich in halite (Iundt, 1971; Edmunds et al., 2003; Kamel et al., 2005; Guendouz and Michelot, 2006; Inoubli et al., 2006; Trabelsi et al., 2009), which buffers the Na/Cl ratio of most samples at ~1. This process is active over the three Tunisian domains. In addition to this, leaching of gypsum/anhydrite and calcite concurs to determine the range of $HCO_3/(Ca + SO_4)$ ratios in groundwaters: sulfate dissolution, which determines a shift of groundwater samples towards the left part of Fig. 10d, appears dominant in Saharan and Eastern domains ($HCO_3/(Ca + SO_4)$ ratios < 0.1); while calcite dissolution (which acts to produce a shift towards the right portion of Fig. 10d), mainly controls water chemistry in the Atlasic Domain

Table 3
Helium isotopes composition of bubbling free gas samples compared to dissolved gas in corresponding groundwaters.

Sample	Site name	Water		Gas			Water		Gas
		$^4He_{xs}$ (ppm)	$^4He_{xs}$ (ppm)	^4He(ppm)	$^4He/^{20}Ne_{meas}$	$^4He_{xs}$ (ppm)	R_{xs}/Ra	R_{xs}/Ra	R_{xs}/Ra
		(1)	(2)				(1)	(2)	
5a	H. Biadha	3.2	4.0	7.8	38.44	7.7	0.262	0.191	0.178
5b	H. Biadha	3.6	3.3	4.9	26.08	4.8	0.179	0.231	0.185
7a	H. Es-Salhine	19.0		32.6	3.43	29.6	0.260		0.245
7b	H. Es-Salhine	22.2	23.5	39.6	3.75	36.2	0.259	0.248	0.129
13a	H. Kef-Ettout	50.3	91.7	46.1	4.01	42.4	0.023	0.060	0.017
13b	H. Kef-Ettout	17.4		40.1	4.12	37.0	0.033		0.028
29	A. Maamar (H. Sollah)	3166	3736	3236	134.76	3228	0.018	0.018	0.022
30	A. Chenama (A. Mouailha)	4141	5161	3023	135.72	3016	0.021	0.023	0.028

In order to compare He concentrations in free gas samples and in corresponding dissolved gas samples, we derived the concentration of the gas phase in equilibrium with each water sample at atmospheric pressure and at the sampling temperature (as given in Table 1). Concentrations are globally in good agreement. However, it must be kept in mind that both water degassing in the hydrothermal system before sampling and/or gas high-pressure in the hydrothermal system inducing higher solubility can play in opposite ways.

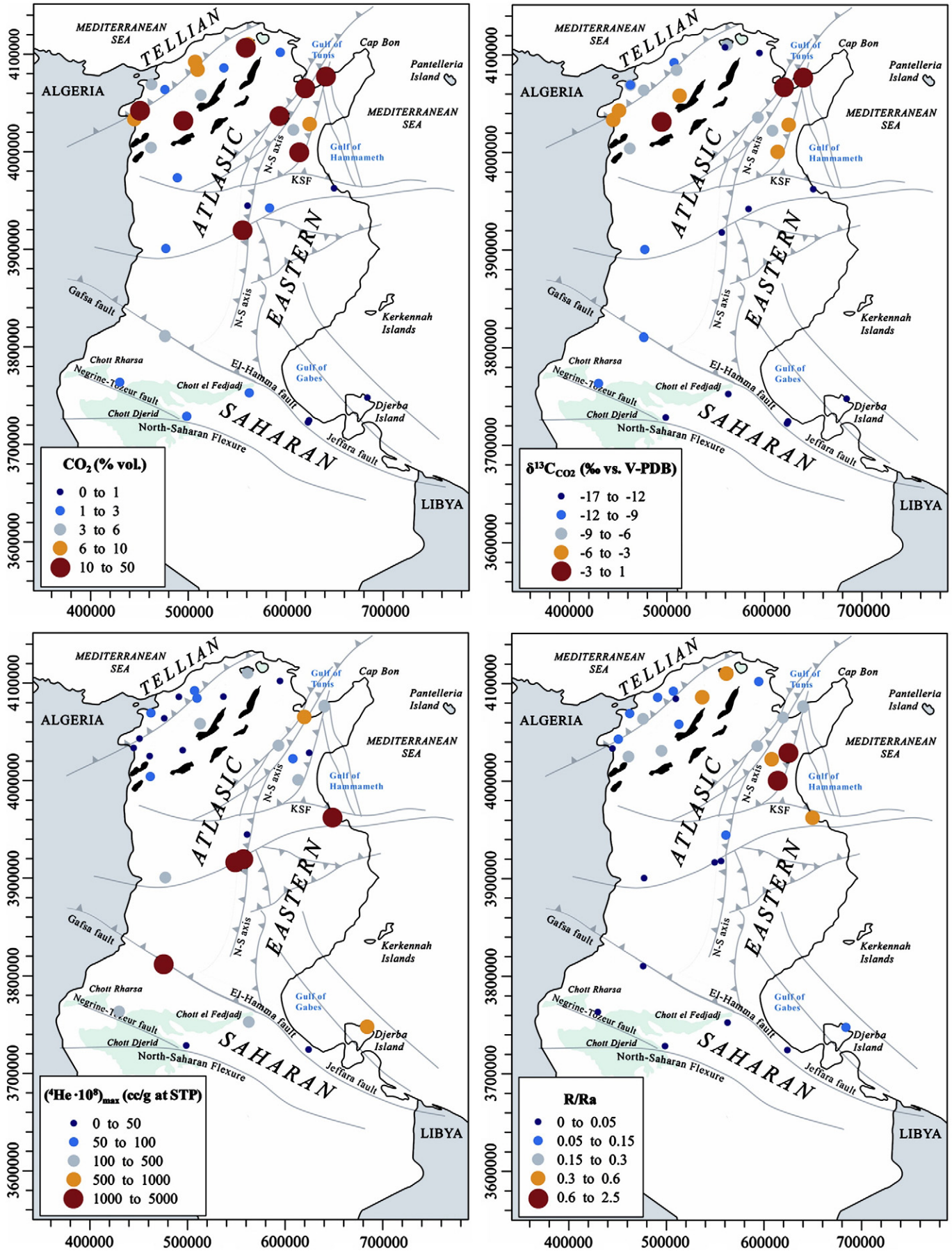

Fig. 8. Maps showing the spatial distribution of CO_2, $\delta^{13}C$, ^4He and R/Ra in Tunisia and their connection to tectonics.

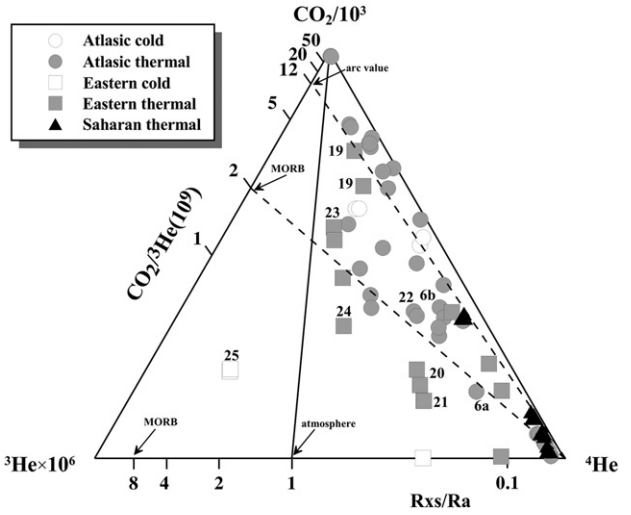

Fig. 9. Ternary plot of CO_2-^{3}He-^{4}He. Solid line represents a mixture of atmospheric He (1Ra) and pure CO_2. Dashed lines represent mixture between radiogenic He and CO_2-^{3}He with average arc ratio (1.2×10^{10}; Sano and Williams, 1996) and average MORB ratio (2×10^9; Marty and Jambon, 1987) respectively.

($HCO_3/(Ca+SO_4)$ ratios>0.1), and more specifically in its Tellian sector (where $HCO_3/(Ca+SO_4)$ ratios occasionally are>1). In the latter area, the absence of halite-bearing formations in the sedimentary succession allows the groundwater Na/Cl ratio to significantly diverge from unity. This Na-excess (relative to Cl) (see samples 3, 8 and 9 in Fig. 10d) likely reflects weathering of feldspars (mainly from sandstones of the Numidian Flysch; Garcia et al., 2001). We cannot exclude, however, that cation exchange processes on mineral surfaces also play a role : these are known to cause a preferential Na-release to weathering solutions at the expense of other cation species (Edmunds et al., 2003; Guendouz et al., 2003; Yermani et al., 2003; Fehdi et al., 2009; Kouzana et al., 2010).

5.2. Origin of carbon and helium

The isotopic compositions of dissolved carbon and helium are known to be sensitive tracers of the origin of volatiles in subsurface fluids. In the following, we examine the possible origin for carbon in the light of the $\delta^{13}C$ composition of the fluids, and the spatial distribution of He isotopes in relation to the structural geology of Tunisia.

5.2.1. Carbon isotopes

The determination of $\delta^{13}C_{TDIC}$ was undertaken to gain insights into the processes controlling the abundance and origin of dissolved carbon in the thermal waters. As shown in Section 4.4, the highly variable carbon isotopic signature of TDIC (Fig. 6a) and CO_2 content (Fig. 6b) point to multiple carbon sources. In the attempt to evaluate the relative contributions from these sources, we follow here the modeling approach developed by Chiodini et al. (2000) to numerically simulate the evolution of the TDIC and $\delta^{13}C_{TDIC}$ of infiltrating meteoric waters in the $CO_{2(g)}$–calcite–water system. The Chiodini et al. (2000) model, developed to investigate the origin of carbon dissolved in groundwaters from the Apennines (Central Italy), stems from the hypothesis that, in tectonically-active sedimentary groundwater systems, the most significant sources of carbon may include : (i) carbonate minerals (all our samples are at equilibrium with calcite as shown by the SI calcite values in Table 1), (ii) organically-derived CO_2 (taken up upon interaction with the organic pool of the soil, or possibly coming from organic carbon buried in deeper geological layers) and, (iii) possibly, deep-rising abiogenic CO_2. The model was numerically solved using the PHREEQC software package (Parkhurst and Appelo, 1999), and the results are reported in Fig. 6.

Two sets of simulations were carried out. In a first set of "biogenic-calcite" model runs, we used as the starting solution an hypothetic rainwater sample having a $TDIC_{rain}$ of $1.48\cdot10^{-5}$ mol·L^{-1} (corresponding to the equilibrium TDIC content in the water-atmospheric CO_2 system at 20 °C and pH = 5.6), and a $\delta^{13}C_{TDIC,rain}$ of −4.88‰ (corresponding to the calculated C-isotopic composition of pure water in equilibrium with atmospheric $CO_{2(g)}$, this having a $\delta^{13}C$ of −7‰) (see Fig. 6a). We then assumed that, upon infiltration, the starting rainwater solution interacts with organically-derived CO_2 ($CO_{2,bio}$) : this process was simulated by addition, in 200 steps, of 0.01 mol of $CO_{2,bio}$ (to 1 kg of water), which isotopic composition ($\delta^{13}CO_{2,bio}$) was varied from −18‰ to −24‰ (Chiodini et al., 2000). At each step, equilibrium with calcite ($\delta^{13}C_{carb}=+2$‰; Chiodini et al., 2000) was imposed (calcite was only allowed to dissolve in – and not to precipitate from – the solution). In the assumption that (i) isotopic equilibrium exists between all of dissolved carbon species, (ii) CO_2 is not degassed from solution (no CO_2 output), and (iii) no isotopic fractionation occurs when CO_2 is added to the initial solution, the TDIC and $\delta^{13}C_{TDIC}$ of model solutions can be calculated using the relations proposed by Wigley et al. (1978). The results of the "biogenic-calcite" model runs are reproduced by the "CO_2(BIO)" solid lines in Figs. 6a,b. These show that, when biogenic CO_2 is added to a calcite-buffered water system, the TDIC contents of model solutions increase at each step, while the respective $\delta^{13}C_{TDIC}$ (Fig. 6a) consistently become more negative. The chemical (χ_{CO2}) and isotopic ($\delta^{13}C_{CO2}$) composition of the gas phase at equilibrium with model solutions, shown in Fig. 6b, evolve following parallel trends towards more ^{13}C-poor compositions. Comparison between modeled trends and measured compositions (Fig. 6a,b) indicates, however, that only a relatively limited number of Tunisian groundwaters (mostly from the CI) can be satisfactorily reproduced by this process; while most of the remaining samples have far more positive $\delta^{13}C_{TDIC}$ and $\delta^{13}C_{CO2}$ values, implying than an additional ^{13}C-rich carbon source must be at play.

A second set of "abiogenic-calcite" model runs was therefore carried out, in which a ^{13}C-rich CO_2 (with $\delta^{13}C$ values ranging from −8 to +4‰) was stepwise added to the starting solution (instead of the ^{13}C-poor biogenic CO_2). As a starting solution for these simulations, we used a moderately C-rich water (indicated by the star in Fig. 6) from one of the "biogenic-calcite" runs: this allows us to account for a small contribution from soil biogenic CO_2 in the first steps of the water infiltration process (sensitivity tests show that the model results are almost unaffected by the choice of the starting solution which contributes indeed to a very low fraction of the total modeled carbon). Again, calcite equilibration was forced at each step of the simulation. Note that the effect of CO_2 degassing (Chiodini et al., 2000; Caliro et al., 2005) on the model runs is not considered here, since this process has negligible effects on the C isotopic balance at the low carbon conditions studied here (stepwise addition of a cumulative CO_2 amount of only 0.03 mol). The model solutions derived from the "abiogenic-calcite" runs, graphically illustrated by the family of dashed lines in Figs. 6a and b, have compositions overlapping the measured TDIC-$\delta^{13}C_{TDIC}$ (χ_{CO2}-$\delta^{13}C_{CO2}$) range for most water samples from the Atlasic and Eastern domains.

Overall, comparison between modeled and natural water compositions clearly highlights that some abiogenic carbon reservoir must be sourcing a relevant fraction of the carbon transported by the Tunisian groundwaters. In order to fit the measured composition of the CO_2-richest Tunisian thermal waters (Fig. 6), this abiogenic CO_2 must be isotopically positive, and most-probably characterized by $\delta^{13}C_{CO2}$ values between 0 and +4‰ vs. V-PDB. This is far beyond the accepted isotopic range of magmatic CO_2, which is comprised between ~−4‰ in the extensional volcanism of Pantelleria (Parello et al., 2000) and −3 to 0‰ in the subduction-related volcanism of Vulcano Island (Capasso et al., 1997) and Etna (Allard et al., 1997;

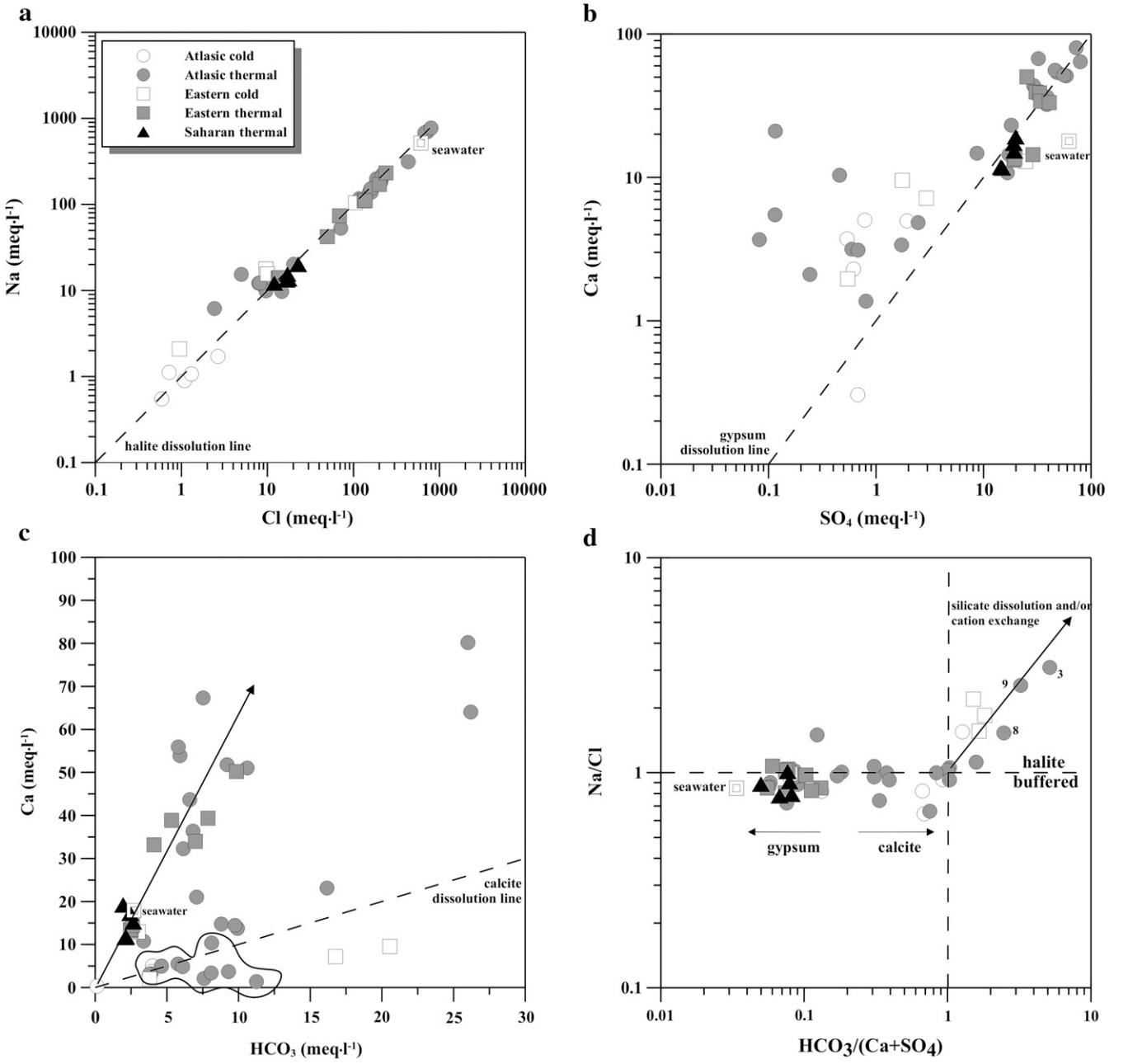

Fig. 10. (a) Na vs. Cl, (b) Ca vs. SO_4, and (c) Ca vs. HCO_3 binary plots of Tunisian groundwaters, showing (as dashed lines) the expected compositions of waters in which halite, gypsum, and calcite are congruently being dissolved. In (c), a white-filled area is used to group a cluster of samples (3, 9–11, 13–14, 20; see Fig. 1) collected on the northernmost part of the Atlasic domain, where calcite dissolution appears as the most significant mineralization process (see also Fig. 3 and related discussion); conversely, a group of samples trends (black arrow) at higher Ca/HCO_3 ratios than expected from calcite dissolution (dashed line), which implies an additional Ca contribution (likely from gypsum/anhydrite dissolution); (d) Na/Cl vs. $HCO_3/(Ca+SO_4)$ diagram, summarizing the key source processes controlling the chemistry of Tunisian groundwaters. See text for explanation.

Chiodini et al., 2011). In addition, we note that our estimated range for abiogenic CO_2 in Tunisia ($\delta^{13}C_{CO2}$ values between 0 and +4‰) is more positive than the estimated deep-CO_2 supply to groundwater systems of central ($\delta^{13}C_{CO2}$ ~−3‰; Chiodini et al., 2000) to north-central Italy ($\delta^{13}C_{CO2}$ from −3 to +1‰; Frondini et al., 2008), where a crustally contaminated mantle has been proposed as the main source of abiogenic CO_2 (Chiodini et al., 2004). Therefore, we argue that metamorphic decarbonation reactions in the deep crust are the most likely source of abiogenic carbon to the Tunisian groundwater system. In fact, assuming a range of $\delta^{13}C$ for Tunisian carbonate rocks of −2 to +2‰ (Charisi and Schmitz, 1995), with an isotope enrichment factor (ε) in the CO_2-calcite system of 0.19 to 2.6‰ in the 200–600 °C temperature range (Bottinga, 1969; Ohmoto and Rye, 1979), we calculate a $\delta^{13}C$ for the CO_2 produced during metamorphic decarbonation (Evans et al., 2008) ranging from −1.81 to 4.6‰, in total agreement with our calculated $\delta^{13}C_{CO2}$ range for Tunisian groundwaters.

The distribution maps of Fig. 8 highlight that this CO_2-rich (Fig. 8a) and ^{13}C-rich (Fig. 8b) volatile component is well represented in the entire northern sector of Tunisia, and more specifically in the northernmost parts of both the Atlasic (Tellian sector) and Eastern domains. This suggests that the intense tectonic activity related to Apennine–Maghrebide orogenesis, and the resulting high geothermal gradients, have likely created the favorable conditions for metamorphic decarbonation reactions to occur at regional scale. While thus the deep crust is likely sourcing the majority of carbon in the area, a striking link between shallow tectonic setting and degassing also clearly emerges, since most CO_2-rich thermal manifestations are discharged in areas where a denser network of active faults (with

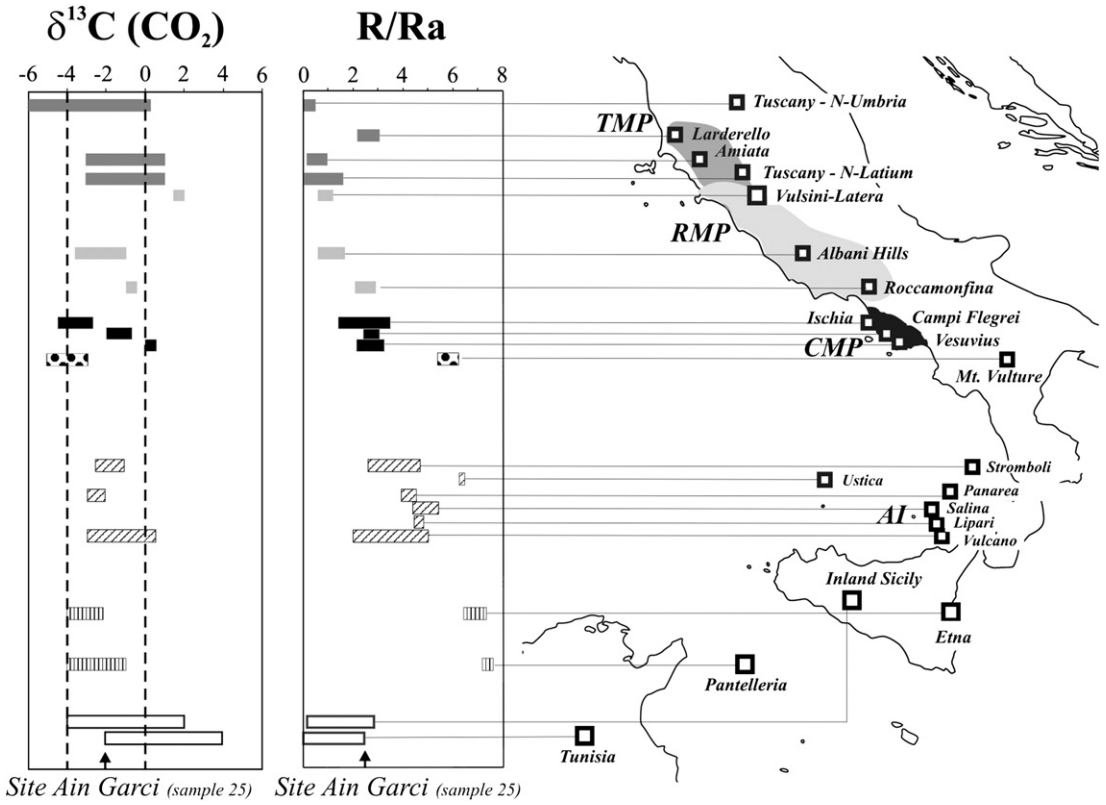

Fig. 11. Central Mediterranean regional North–south trend for $^3He/^4He$ ratios (expressed as R/Ra) and $\delta^{13}C$, from Tuscany to the Pantelleria Rift and Tunisia. *Tuscany magmatic province (TMP)*: data from Hooker et al. (1985); Minissale et al. (1997); Chiodini et al. (2000); Italiano et al. (2001); Minissale (2004); Frondini et al. (2008, 2009). *Roman magmatic province (RMP)*: data from Minissale et al. (2000); Chiodini and Frondini (2001); Martelli et al. (2004); Chiodini et al. (2007). *Campanian magmatic province (CMP)*: data from Inguaggiato et al. (2000); Chiodini et al. (2001); Federico et al. (2002); Martelli et al. (2004); Caliro et al. (2005, 2007); Di Napoli et al. (2009). *Mt. Vulture*: data from Paternoster (2004) and Caracausi et al. (2009). *Aeolian Island (AI)*: data from Capasso et al. (1997, 2005); Tedesco and Scarsi (1999); Caliro et al. (2004); Caracausi et al. (2005); Martelli et al. (2008). *Ustica*: data from Martelli et al. (2008). *Etna*: data from Allard et al. (1997); D'Alessandro et al. (1997). *Inland Sicily*: data from Caracausi et al. (2005) and Grassa et al. (2006). *Tunisia*: this work.

clear surface expression) favors the ascent of the deeply produced gasses.

In spite of the apparent prevailing crustal derivation of carbon, we acknowledge however that some extent of mantle CO_2 contribution may also exist locally. In particular, sample 25 (Aïn Garci) has unusually $\delta^{13}C_{CO2}$-poor composition ($\delta^{13}C_{CO2} = -5.7‰$), at least relatively to similarly CO_2-rich samples (e.g., sample 4, $\delta^{13}C_{CO2} = -4.3‰$). This may be consistent with a contribution from some isotopically lighter abiogenic CO_2. Since sample 25 has also an unusually high He isotope composition (R/Ra = 2.4), we conclude that some mantle-derived CO_2 input has to be considered for the Eastern Tunisian domain.

5.2.2. Helium isotopes distribution: links with geodynamics

Helium results reveal some interesting spatial trends in the helium isotope composition (Fig.8c and d). Not unexpectedly, the lowest $(^3He/^4He)_{xs}$ values (0.01–0.02 Ra) are observed along an east−west Gabes–Tozeur line, associated with the old groundwaters of the CI aquifer. These $^3He/^4He$ values are comparable to the crustal production ratio (Ballentine and Burnard, 2002), with no detectable amount of mantle-derived ^3He added to this huge continental groundwater mass. This is in agreement with previous studies of helium isotopes in sedimentary basin, which conclude that tectonically-stable regions are essentially impermeable to mantle volatiles (Oxburgh et al., 1986; Marty et al., 2003; Kulongoski et al., 2008). In contrast with the $^3He/^4He$ ratios which are quite homogeneous, helium concentrations are more heterogeneous (Fig. 8c), ranging from 19.9×10^{-8} cm^3STP/g in the Ras-el-Ain borehole (sample 38) to 404.8×10^{-8} cm^3STP/g in El-Hamma (sample 39). This heterogeneity may be due to subsurface channeling of the crustal helium flux along discontinuities such as the El Hamma fault (Fig. 1). Further east, approaching the Gulf of Gabès and the island of Jerba, the $(^3He/^4He)_{xs}$ values rise up to 0.11 Ra. Although the region is characterized by large scale mixing between the CI groundwaters and the upper Djeffara local aquifer (Trabelsi et al., 2009), this cannot explain the higher air-corrected $^3He/^4He$ values, which may indeed be linked to the regional mantle-^3He anomaly observed along the oriental margin of Tunisia, associated with the Sahel-Pelagian Block (see discussion below).

The low $^3He/^4He$ domain is not restricted to the Saharan Platform but actually extends to the entire Atlasic domain of central Tunisia (Fig. 8d). This Atlasic domain displays the highest helium concentrations : along the Gafsa Fault, helium concentrations of 1777 and 4723×10^{-8} cm^3STP/g (the highest value of our data set) are observed in the two production wells (Z3 and Z1 respectively) of Sidi Ahmed Zarrouk (samples 34–35). High helium concentrations are also recorded southwest of Kairouan, in the two nearby sites of Ain Maamar (sample 29) (2760×10^{-8} cm^3STP/g) and Ain Chenama (sample 30) (4060×10^{-8} cm^3STP/g) both characterized by vigorous surface bubbling and high CO_2 and methane contents. This high helium flux is associated with the tectonic knot at the intersection of the N–S Axis and the Mhrila–Cherichira fault zone — MCF (Fig. 1; Martinez et al., 1990; El Ghali et al., 2003). This again emphasizes the role of deep tectonic controls in channeling up and transporting deep crustal volatiles to shallow levels.

Northwards, low $^3He/^4He$ values between 0.02 and 0.05 Ra extend to the latitude of El Kef (sample 1). Further north, hot springs are more numerous and their $^3He/^4He$ ratios tend to increase significantly (although in some places $^3He/^4He$ values remain close to the crustal

ratio) : $(^3He/^4He)_{xs} = 0.13 \pm 0.08$ Ra for the cluster of hot springs located in the northwestern part of Tunisia, and up to 0.4 Ra for the Ichkeul group (samples 15, 16 and 17) located at the extreme north of the country. This increase in the number of geothermal manifestations, accompanied by the presence of a weak but significant (5%) mantle helium component (see Fig. 7), should be put in relation with the relatively high level of seismic activity across the whole area (Gueddiche et al., 1998), which could favor water circulation and mantle–helium leakage along active faults.

The eastern part of Tunisia displays higher $(^3He/^4He)_{xs}$ values (Fig. 8d) indicative of a substantial mantle volatile input. The highest (and sole value above the atmospheric ratio −2.4 Ra) is recorded in the carbogaseous mineral water of Ain Garci (sample 25), in possible relation with the nearby volcanic outcrops of Djebel Fadeloun and Djebel Abid. Other $(^3He/^4He)_{xs}$ values range from 0.3 Ra to 0.65 Ra. The uppermost values (0.6 Ra and 0.65 Ra) correspond to the two sites nearest to Ain Garci (sample 25), suggesting the presence of a regional mantle ^3He anomaly. Helium concentrations range from 20 to 3800×10^{-8} cm^3 STP/g, the latter being recorded in the abandoned well of Sidi Abdelhamid (sample 26) located on a major tectonic accident, the Kairouan–Sousse Fault (KSF) (Khomsi et al., 2004). Eastern Tunisia has been affected by an important tectonic activity since the Mesozoic times, with multiple magmatic intrusions (Mattoussi Kort et al., 2005). This northeastern part of the African plate, commonly referred to as the Pelagian Block (Burollet, 1978), extends from Tunisia to Sicily, and is thought as the southernmost foreland of the Apennine–Maghrebide orogenic system (Tavarnelli et al., 2004). This area is characterized by strong extensional tectonics (Pantelleria rift zone), crustal thinning, and present-day magmatic activity with $(^3He/^4He)$ ratios around 8 Ra, typical of the upper mantle (Parello et al., 2000). This lithospheric stretching and decompression melting in the central portion of the Pelagian Block may facilitate the transport of mantle helium through the thinned crust away from the rift zone across the existing network of fractures and deep faults.

6. Concluding remarks

The chemical analysis of Tunisian groundwaters highlights the heterogeneity of the mineralization processes at work in Tunisia, as a consequence of the extremely variable geological and tectonic features. In terms of chemical composition, we conclude that dissolution of halite and gypsum plays a key control on groundwater chemistry. With respect to carbon and helium, this study represents the first isotopic characterization of Tunisian hydrothermal manifestations. Helium and carbon isotope systematics confirm the predominantly crustal origin for the gas phase supply to the Tunisian geothermal aquifers. Most samples are indeed characterized by radiogenic-type helium associated with a CO_2 either predominantly organic (in the Saharan domain) or metamorphic in origin (in the Atlasic domain). As a whole, volatiles in Tunisian thermal fluids have He isotopic signatures resembling those characteristic of natural fluids from the northern Apennine area (Tuscany and N-Umbria), which are external to the Pleistocene Italian magmatic provinces, and which consistently have a prevalent crustal gas signature (Minissale et al., 2000). The prevalent crustal derivation of the fluids in most part of Tunisia is consistent with the absence of recent magmatism in the area (latest magmatic activity in Tunisia dates back to Miocene, related to the convergence between Africa and Eurasia). In eastern Tunisia, however, helium isotopes definitely support a more mantle-like derivation for He and CO_2. In particular, the Ain Garci area is characterized by substantially higher helium isotopic compositions (up to 2.4 Ra, corresponding to 30% of mantle-derived helium), and by more negative isotopic composition of the dissolved carbon, consistent with a contribution from a lighter ($\delta^{13}C \sim -2$ to 0‰) CO_2 source. That mantle volatiles are to some extent involved in the eastern part of Tunisia would indeed be consistent with the fact that the Pelagian Block (which eastern Tunisia is part of) has been deeply affected by extensional and transtensional tectonics since the opening of the Tethys Ocean (Tavarnelli et al., 2004), a process which is still ongoing in the Sicily Channel.

Our results add a new piece in the puzzle of the regional variability of deep fluid contributions in the western Mediterranean. Fig. 11 extends to Northern Africa the regional (N to S) isotopic trends, originally derived from the analysis of a variety of fluid types (natural gas discharges, dissolved gasses in groundwater, fluid inclusions in volcanic rocks) collected from seismically or volcanically active districts of northern-central (Tuscany) to southern (Sicily) Italy (Parello et al., 2000; Martelli et al., 2004, 2008). It shows that the Italian mantle gas anomaly only marginally extends to northwestern Africa, and that the north to south trend of increasing R/Ra ratios, from the Tuscany, Roman and Campanian Magmatic Provinces ($^3He/^4He$ <3 Ra) to Etna and Pantelleria ($^3He/^4He \sim 7$Ra), via the Aeolian Islands ($^3He/^4He \sim 3$–5 Ra), apparently comes to an end at the latitude of the Pantelleria Rift. Our study finally strengthens the earlier conclusions of Mahood and Hildreth (1983) on the exceptional nature of Pantelleria volcanism, confirming that crustal thinning in the Sicily channel is unambiguously acting as a preferential path for upper mantle degassing at the regional scale.

Acknowledgments

This work benefited from the financial support of CNRS-DGRS (project no. 22636). We would like to thank the Tunisian Office of Thermalism for its cooperation and support. We also thank Sonia Falourd and Benedicte Minster for the water isotope measurements.

References

Aiuppa, A., Giudice, G., Gurrieri, S., Liuzzo, M., Burton, M., Caltabiano, T., McGonigle, A.J.S., Salerno, G., Shinohara, H., Valenza, M., 2008. Total volatile flux from Mount Etna. Geophys. Res. Lett. 35 (24), L24302 art. no.

Allard, P., Carbonelle, J., Dajlevic, D., Le Bronec, J., Morel, P., Robe, M.C., Maurenas, J.M., Faivre-Pierret, R., Martin, D., Sabroux, J.C., Zettwoog, P., 1991. Eruptive and diffuse emissions of CO_2 from Mount Etna. Nature 351, 387–391.

Allard, P., D'Alessandro, W., Jean-Baptiste, P., Parello, F., Parisi, B., Flehoc, C., 1997. Mantle-derived helium and carbon in groundwaters and gas emanations of Mount Etna. Italy. Earth Planet. Sci. Lett. 148, 501–516.

Ballentine, C.J., Burnard, P.G., 2002. Production, release and transport of noble gases in the continental crust. In: Porcelli, D., Ballentine, C.J., Wieler, R. (Eds.), Noble gases in geochemistry and cosmochemistry: Rev. Mineral. Geochem., 47, pp. 481–538.

Ballentine, C.J., O'Nions, R.K., Oxburgh, E.R., Horvath, F., Deak, J., 1991. Rare-gas constraints on hydrocarbon accumulation, crustal degassing and groundwater-flow in the Pannonian Basin. Earth Planet. Sci. Lett. 105, 229–246.

Ballentine, C.J., Burgess, R., Marty, B., 2002. Tracing fluid origin, transport and interaction in the crust. In: Porcelli, D., Ballentine, C.J., Wieler, R. (Eds.), Noble gases in geochemistry and cosmochemistry: Rev. Mineral. Geochem., 47, pp. 539–614.

Bédir, M., 1995. Mécanismes géodynamiques des bassins associés aux couloirs de coulissement de la marge atlasique de la Tunisie. Thèse Doc. Etat, Tunis II, Tunisia, 416 pp.

Bédir, M., 1999. Subsurface structuring of the Eastern Mediterranean Tunisian basins: CIESM Workshop Series, 6, pp. 81–85.

Ben Ferjani, A., Burollet, P.F., Mejri, F., 1990. Petroleum Geology of Tunisia. Mem. E. T. A. P., vol. 1. Tunis, Tunisia. 194 pp.

Bishop, W.F., 1975. Geology of Tunisia and adjacent parts of Algeria and Lybia. Am. Assoc. Pet. Geol. Bull. 59, 413–450.

Bottinga, Y., 1969. Calculated fractionation factors for carbon and hydrogen isotope exchange in system calcite–carbon dioxide–graphite–methane–hydrogen–water vapor. Geochim. Cosmochim. Acta 33, 49–64.

Bouaziz, S., Barrier, E., Soussi, M., Turki, M., Zouari, H., 2002. Tectonic evolution of the northern african margin in Tunisia from paleostress data and sedimentary record. Tectonophysics 357, 227–253.

Bourg, C., Stievenard, M., Jouzel, J., 2001. Hydrogen and oxygen isotopic composition of aqueous salt solutions by gas–water equilibration method. Chem. Geol. 173, 331–337.

Bouri, S., Makni, J., Ben, Dhia H., 2008. A synthetic approach integrating surface and subsurface data for prospecting deep aquifers : the Southeast Tunisia. Environ. Geol. 54, 1473–1484.

Brook, G.A., Folkoff, M.E., Box, E.O., 1983. A global model of soil carbon dioxide. Earth Surf. Processes Landforms 8, 79–88.

Burollet, P.F., 1956. Contribution à l'étude stratigraphique de la Tunisie centrale. Ann. Mines Geol., 18. Tunis, Tunisia. 345 pp.

Burollet, P.F., 1978. Quaternary and recent movements in Kerkennah Island (Tunisie orientale). C.R. Acad. Sci., 286. Série D, Paris, pp. 1133–1136.
Caliro, S., Caracausi, A., Chiodini, G., Ditta, M., Italiano, F., Longo, M., Minopoli, C., Nuccio, P.M., Paonita, A., Rizzo, A., 2004. Evidence of a new magmatic input to the quiescent volcanic edifice of Panarea, Aeolian Islands. Italy. Geophys. Res. Lett. 31, 1–5.
Caliro, S., Chiodini, G., Avino, R., Cardellini, C., Frondini, F., 2005. Volcanic degassing at Somma-Vesuvio (Italy) inferred by chemical and isotopic signatures of ground-water. Appl. Geochem. 20 (6), 1060–1076.
Caliro, S., Chiodini, G., Moretti, R., Avino, R., Granieri, D., Russo, M., Fiebig, J., 2007. The origin of the fumaroles of La Solfatara (Campi Flegrei, South Italy). Geochim. Cosmochim. Acta 71, 3040–3055.
Capasso, G., Inguaggiato, S., 1998. A simple method for the determination of dissolved gases in natural waters. An application to thermal waters from Vulcano Island. Appl. Geochem. 13, 631–642.
Capasso, G., Favara, R., Inguaggiato, S., 1997. Chemical features and isotopic composition of gaseous manifestations on Vulcano Island, Aeolian Islands, Italy: an interpretative model of fluid circulation. Geochim. Cosmochim. Acta 61, 3425–3440.
Capasso, G., Favara, R., Inguaggiato, S., 2000. Interaction between fumarolic gases and thermal groundwaters at Vulcano Island (Italy): evidences from chemical composition of dissolved gases in waters. J. Volcanol. Geotherm. Res. 102, 309–318.
Capasso, G., Carapezza, M.L., Federico, C., Inguaggiato, S., Rizzo, A., 2005. Geochemical monitoring of the 2002–2003 eruption at Stromboli volcano (Italy): precursory changes in the carbon and helium isotopic composition of fumarole gases and thermal waters. Bull. Volcanol. 68, 118–134.
Caracausi, A., Favara, R., Italiano, F., Nuccio, P.M., Paonita, A., Rizzo, A., 2005. Active geodynamics of the central Mediterranean Sea: tensional tectonic evidences in western Sicily from mantle-derived helium. Geophys. Res. Lett. 32, L04312. doi:10.1029/2004GL021608.
Caracausi, A., Nuccio, P.M., Favara, R., Nicolosi, M., Paternoster, M., 2009. Gas hazard assessment at the Monticchio crater lakes of Mt. Vulture, a volcano in Southern Italy. Terra Nova 21, 83–87.
Castany, G., 1982. Bassin sédimentaire du Sahara septentrional (Algérie-Tunisie)—Aquiféres du continental intercalare et du complexe terminal. Bull. Bur. Rec. Géol. Min. (BRGM) Sér. 2 (3), 127–147.
Celle-Jeanton, H., Zouari, K., Travi, Y., Daoud, A., 2001. Caractérisation isotopique des pluies en Tunisie. Essai de typologie dans la région de Sfax. C.R. Acad. Sci., 333. Séries IIA, Paris, pp. 625–631.
Charisi, S.D., Schmitz, B., 1995. Stable ($\delta^{13}C$, $\delta^{18}O$) and strontium ($^{87}Sr/^{86}Sr$) isotopes through the Paleocene at Gebel Aweina, eastern Tethyan region. Palaeogeogr. Palaeoclimatol. Palaeoecol. 116, 103–129.
Chiodini, G., Frondini, F., 2001. Carbon dioxide degassing from the Albani Hills volcanic region, Central Italy. Chem. Geol. 177, 67–83.
Chiodini, G., Frondini, F., Cardellini, C., Parello, F., Peruzzi, L., 2000. Rate of diffuse carbon dioxide degassing estimated from carbon balance of regional aquifers: the case of central Apennine. Italy. J. Geophys. Res. 105, 8423–8434.
Chiodini, G., Marini, L., Russo, M., 2001. Geochemical evidences of high temperature hydrothermal brines at Vesuvio volcano (Italy). Geochim. Cosmochim. Acta 65, 2129–2147.
Chiodini, G., Cardellini, C., Amato, A., Boschi, E., Caliro, S., Frondini, F., Ventura, G., 2004. Carbon dioxide Earth degassing and seismogenesis in central and southern Italy. Geophys. Res. Lett. 31, L07615. doi:10.1029/2004GL019480.
Chiodini, G., Baldini, A., Barberi, F., Carapezza, M.L., Cardellini, C., Frondini, F., Granieri, D., Ranaldi, M., 2007. Carbon dioxide degassing at Latera caldera (Italy): evidence of geothermal reservoir and evaluation of its potential energy. J. Geophys. Res. 112, B12204. doi:10.1029/2006JB004896.
Chiodini, G., Caliro, S., Cardellini, C., Avino, R., Granieri, D., Schmidt, A., 2008. Carbon isotopic composition of soil CO_2 efflux, a powerful method to discriminate different sources feeding soil CO_2 degassing in volcanic-hydrothermal areas. Earth Planet. Sci. Lett. 274, 372–379.
Chiodini, G., Caliro, S., Aiuppa, A., Avino, R., Granieri, D., Moretti, R., Parello, F., 2011. First $^{13}C/^{12}C$ isotopic characterisation of volcanic plume CO_2. Bull. Volc. 73, 531–542. doi:10.1007/s00445-010-0423-2, in press.
Cornet, A., 1964. Introduction à l'hydrogéologie saharienne. Rev. Geog. Phys. Geol. Dyn. 6, 5–72.
Craig, H., 1961. Standards for reporting concentrations of deuterium and oxygen-18 in natural waters. Science 133, 1833–1834.
D'Alessandro, W., De Gregorio, S., Dongarrà, G., Gurrieri, S., Parello, F., Parisi, B., 1997. Chemical and isotopic characterization of the gases of Mount Etna (Italy). J. Volcanol. Geotherm. Res. 78, 65–76.
De Leeuw, G.A.M., Hilton, D.R., Fisher, T.P., Walker, J.A., 2007. The He–CO_2 isotope and relative abundance characteristics of geothermal fluids in El Salvador and Honduras: new constraints on volatile mass balance of the Central American Volcanic Arc. Earth Planet. Sci. Lett. 258, 132–146.
Deines, P., Langmuir, D., Harmon, R.S., 1974. Stable carbon isotope ratios and the existence of a gas phase in the evolution of carbonate groundwater. Geochim. Cosmochim. Acta 38, 1147–1164.
Di Napoli, R., Aiuppa, A., Bellomo, S., Brusca, L., D'Alessandro, W., Candela, E., Longo, M., Pecoraino, G., Valenza, M., 2009. A model for Ischia hydrothermal system: evidences from the chemistry of thermal groundwaters. J. Volcanol. Geotherm. Res. 186, 133–159.
Edmunds, W.M., Guendouz, A.H., Mamou, A., Moula, A., Shand, P., Zouari, K., 2003. Groundwater evolution in the Continental Intercalaire aquifer of southern Algeria and Tunisia: trace element and isotopic indicators. Appl. Geochem. 18, 805–822.
El Ghali, A., Bobier, C., Ben Ayed, N., 2003. Rôle du système de faille E–W dans l'évolution géodynamique de l'avant-pays de la chaîne alpine de Tunisie. Exemple de l'accident de Sbiba-Chérichira en Tunisie centrale. Bull. Soc. Geol. Fr. 174 (4), 373–381.
Evans, M.J., Derry, L.A., France-Lanord, C., 2008. Degassing of metamorphic carbon dioxide from the Nepal Himalaya. Geochem. Geophys. Geosyst. 9, Q04021. doi:10.1029/2007GC001796.
Favara, R., Grassa, F., Inguaggiato, S., Pecoraino, G., Capasso, G., 2002. A simple method to determine the $\delta^{13}C$ of total dissolved inorganic carbon. Geofis. Int. 41, 313–320.
Federico, C., Aiuppa, A., Allard, P., Bellomo, S., Jean-Baptiste, P., Parello, F., Valenzia, M., 2002. Magma-derived gas influx and water–rock interactions in the volcanic aquifer of Mt Vesuvius. Italy. Geochim. Cosmochim. Acta 66, 963–981.
Fehdi, Ch., Rouabhia, Aek, Baali, F., Boudoukha, A., 2009. The hydrogeochemical characterization of Morsott-El Aouinet aquifer, Northeastern Algeria. Environ. Geol. 58, 1611–1620.
Frondini, F., Caliro, S., Cardellini, C., Chiodini, G., Morgantini, N., Parello, F., 2008. Carbon dioxide degassing from Tuscany and Northern Latium (Italy). Glob. Planet. Chang. 61, 89–102.
Frondini, F., Caliro, S., Cardellini, C., Chiodini, G., Morgantini, N., 2009. Carbon dioxide degassing and thermal energy release in the Monte Amiata volcanic-geothermal area (Italy). Appl. Geochem. 24, 860–875.
Gabtni, H., Jallouli, C., Mickus, K., Zouari, H., Turki, M.M., 2005. Geophysical Constraints on the location and nature of the North Saharan Flexure in Southern Tunisia. Pure Appl. Geophys. 162, 2051–2069.
Garcia, M.G., Del Hidalgo, M., Blesa, M.A., 2001. Geochemistry of groundwater in the alluvial plain of Tucuman province Argentina. J. Hydrol. 9, 597–610.
Gat, S.R., Carmi, I., 1970. Evolution of the isotopic composition of atmospheric waters in the Mediterranean sea area. J. Geophys. Res. 75, 3039–3048.
Giggenbach, W.F., 1988. Geothermal solute equilibria. Derivation of Na–K–Mg–Ca geoindicators. Geochim. Cosmochim. Acta 52, 2749–2765.
Giggenbach, W.F., Sano, Y., Wakita, H., 1993. Isotopic composition of helium, and CO_2 and CH_4 contents in gases produced along the New Zealand part of a convergent plate boundary. Geochim. Cosmochim. Acta 57, 3427–3455.
Goff, F., Janik, C.J., 2000. Geothermal systems. In: Sigurdsson, H., Houghton, B., McNutt, S., Rymer, H., Stix, J. (Eds.), Encyclopedia of Volcanoes. Academic Press, San Diego, CA, pp. 817–834.
Gonfiantini, R., Conrad, G., Fontes, JCh., Sauzay, G., Payne, B.R., 1974. Etude isotopique de la nappe du Continental Intercalaire et de ses relations avec les autres nappes du Sahara septentrional (Isotopic investigation of the Continental Intercalaire aquifer and its relationship with other aquifers in the northern Sahara). Isotope Techniques in Groundwater Hydrology, vol. 1. IAEA SM-182/25, Vienna, pp. 227–241.
Graham, D.W., 2002. Noble gas isotope geochemistry of Mid-Ocean Ridge and Ocean Island Basalts: characterization of mantle source reservoirs. In: Porcelli, D., Ballentine, C.J., Wieler, R. (Eds.), Noble gases in geochemistry and cosmochemistry: Rev. Mineral. Geochem., 47, pp. 247–317.
Grassa, F., Capasso, G., Favara, R., Ingaggiato, S., 2006. Chemical and isotopic composition of waters and dissolved gases in some thermal springs of Sicily and adjacent volcanic islands. Italy. Pure Appl. Geophys. 163, 781–807.
Griesshaber, E., O'Nions, R.K., Oxburgh, E.R., 1992. Helium and carbon isotope systematics in crustal fluids from the Eiffel, the Rhine Graben and Black Forest. Chem. Geol. 99, 213–235.
Gueddiche, M., Ben Ayed, N., Mohammadioun, G., Mohammadioun, B., Elghali, A., Chekhma, H., Diament, M., Dubois, J., 1998. Etude sismotectonique de la Tunisie nord-orientale. Bull. Soc. Geol. Fr. 169, 789–796.
Guendouz, A., Michelot, J.L., 2006. Chlorine-36 dating of deep groundwater from northern Sahara. J. Hydrol. 328, 572–580.
Guendouz, A., Moulla, A.S., Edmunds, W.M., Shand, P., Zouari, K., Mamou, A., 1997. Palaeoclimatic information contained in groundwaters of the Grand Erg Oriental, North Africa. Int Symp Isotope Techniques in the Study of Past and Current Environmental Changes in the Hydrosphere and Atmosphere, Vienna, 14–18 April 1997. IAEA-SM-349-/43.
Guendouz, A., Moulla, A.S., Edmunds, W.M., Zouari, K., Shand, P., Mamou, A., 2003. Hydrogeochemical and isotopic evolution of water in the Complex Terminal aquifer in the Algerian Sahara. Hydrogeol. J. 11, 483–495.
Güleç, N., Hilton, D.R., Mutlu, H., 2002. Helium isotope variations in Turkey: relation to tectonics, volcanism and recent seismic activities. Chem. Geol. 187, 129–142.
Hamada and Tanaka, 2001. Dynamics of carbon dioxide in soil profiles based on long-term field observation. Hydrol. Process. 15, 1829–1845.
Hilton, D.R., 1996. The helium and carbon isotope systematics of a continental geothermal system: results from monitoring studies at Long Valley caldera (California, USA). Chem. Geol. 127, 269–295.
Hilton, D.R., Fischer, T.P., Marty, B., 2002. Noble gases and volatile recycling at subduction zones. In: Porcelli, D., Ballentine, C.J., Wieler, R. (Eds.), Noble gases in geochemistry and cosmochemistry: Rev. Mineral. Geochem., 47, pp. 319–370.
Hooker, P.J., Bertrami, R., Lombardi, S., O'Nions, R.K., Oxburgh, E.R., 1985. Helium-3 anomalies and crust-mantle interactions in Italy. Geochim. Cosmochim. Acta 49, 2505–2513.
Hulston, J.R., Hilton, D.R., Kaplan, I.R., 2001. Helium and carbon isotope systematics of natural gases from Taranaki Basin, New Zealand. Appl. Geochem. 16, 419–436.
Inguaggiato, S., Pecoraino, G., D'Amore, F., 2000. Chemical and isotopic characterization of fluid manifestations of Ischia Island. J. Volcanol. Geotherm. Res. 99, 151–178.
Inoubli, N., Gouasmia, M., Gasmi, M., Mhamdi, A., Ben Dhia, H., 2006. Integration of geological, hydrochemical and geophysical methods for prospecting thermal water resources: The case of the Hmeïma region (Central –Western Tunisia). J. Afr. Earth. Sci. 46, 180–186.

Irwin, W.P., Barnes, I., 1980. Tectonic relations of carbon dioxide discharges and earthquakes. J. Geophys. Res. 85, 3115–3121.
Italiano, F., Martinelli, G., Nuccio, P.M., 2001. Anomalies of mantle-derived helium during the 1997–1998 seismic swarm of Umbria-Marche. Italy. Geophys. Res. Lett. 28, 839–842.
Iundt, F., 1971. Potentiel géothermique de la Tunisie. Etude géochimique. Bureau de Recherches Géologiques et Minières. Service Géologique National, Orléans, France.
Jean-Baptiste, P., Mantisi, F., Dapoigny, A., Stievenard, M., 1992. Design and performance of a mass spectrometric facility for measuring helium isotopes in natural waters and for low-level tritium determination by the ^{3}He ingrowth method. Appl. Radiat. Isot. 43, 881–891.
Jellouli, A., 2002. La Tunisie thermale. Office du thermalisme, Tunis. 193 pp.
Kamel, S., Dessi, L., Zouari, K., Abidi, B., 2005. Geochemical and isotopic investigation of the aquifer system in the Djerid-Nefzaoua basin, southern Tunisia. Environ. Geol. 49, 159–170.
Khomsi, S., Bédir, M., Zouari, H., Ben Jemia, G., 2004. Mise en évidence et analyse d'une structure atlasique ennoyée au front de la Chaîne alpine tunisienne. C.R. Geosci. 336, 1293–1300.
Khomsi, S., Bédir, M., Soussi, M., Ben Jemia, G., Ben Ismail-Lattrache, K., 2007. Réponse au commentaire de N. Brahim et E. Mercier à propos de l'article de S. Khomsi et al. C.R. Geoscience 338 (1–2) (2006) 41–49. C.R. Geoscience 339, 173–177.
Kipfer, R., Aeschbach-Hertig, W., Peeters, F., Stute, M., 2002. Noble gases in lakes and ground waters. In: Porcelli, D., Ballentine, C.J., Wieler, R. (Eds.), Noble gases in geochemistry and cosmochemistry: Rev. Mineral. Geochem., 47, pp. 615–700.
Kouzana, L., Ben Mammou, A., Sfar Felfoul, M., 2009. Seawater intrusion and associated processes: case of the Korba aquifer (Cap Bon, Tunisia). C.R. Geosci. 341, 21–35.
Kouzana, L., Benassi, R., Ben Mammou, A., Sfar Felfoul, M., 2010. Geophysical and hydrochemical study of the seawater intrusion in Mediterranean semi arid zones. Case of the Korba coastal aquifer (Cap-Bon, Tunisia). J. Afr. Earth. Sci. 58, 242–254.
Kulongoski, J.T., Hilton, D.R., Cresswell, R.G., Hostetler, S., Jacobson, G., 2008. Helium-4 characteristics of groundwaters from Central Australia : comparative chronology with Chlorine-36 and Carbon-14 dating techniques. J. Hydrol. 348, 176–194.
Laaridhi-Ouazaa, N., 1994. Etude minéralogique et géochimique des épisodes magmatiques mésozoïques et miocénes de la Tunisie. Thèse Doc. Etat, Univ. Tunis II, Tunisia, 466 pp.
Langelier, W.F., Ludwig, H.F., 1942. Graphical method for indicating the mineral character of natural waters. J. Am. Waterworks Assoc. 34, 335–352.
Lollar, B.S., Ballentine, C.J., 2009. Insights into deep carbon derived from noble gases. Nat. Geosci. 2, 543–547.
Lollar, B.S., Ballentine, C.J., ONions, R.K., 1997. The fate of mantle-derived carbon in a continental sedimentary basin: integration of C/He relationships and stable isotope signatures. Geochim. Cosmochim. Acta 61, 2295–2307.
Mahood, G.A., Hildreth, W., 1983. Nested calderas and trapdoor uplift at Pantelleria, Strait of Sicily. Geology 11, 722–726.
Martelli, M., Nuccio, P.M., Stuart, F.M., Burgess, R., Ellam, R.M., Italiano, F., 2004. Helium–strontium isotope constraints on mantle evolution beneath the Roman Comagmatic Province. Italy. Earth Planet. Sci. Lett. 224, 295–308.
Martelli, M., Nuccio, P.M., Stuart, F.M., Di Liberto, V., Ellam, R.E., 2008. Constrains on mantle source and interactions from He–Sr isotope variation in Italian Plio-Quaternary volcanism. Geochem. Geophys. Geosyst. 9, Q02001. doi:10.1029/2007GC001730.
Martinez, C., Andrieux, J., Truillet, R., Ben Jemiaa, M., 1990. Les structures synsédimentaires miocènes en compression associées au décrochement dextre Mhrila-Chérichira (Tunisie centrale). Bull. Soc. Geol. Fr. 6 (1), 167–176.
Marty, B., Jambon, A., 1987. C/^{3}He in volatile fluxes from the solid earth : implication for carbon geodynamics. Earth Planet. Sci. Lett. 83, 16–26.
Marty, B., Gunnlaugsson, E., Jambon, A., Oskarsson, N., Ozima, M., Pineau, F., Torssander, P., 1991. Gas geochemistry of geothermal fluids, the Hengill area, southwest rift zone of Iceland. Chem. Geol. 91, 207–225.
Marty, B., O'Nions, R.K., Oxburgh, E.R., Martel, D., Lombardi, S., 1992. Helium isotopes in Alpine regions. Tectonophysics 206, 1–8.
Marty, B., Pik, R., Gezahegn, Y., 1996. Helium isotopic variations in Ethiopian plume lavas: nature of magmatic sources and limit on lower mantle contribution. Earth Planet. Sci. Lett. 144, 223–237.
Marty, B., Dewonck, S., France-Lanord, C., 2003. Geochemical evidence for efficient aquifer isolation over geological timeframes. Nature 425, 55–58.
Mata, J., Moreira, M., Doucelance, R., Ader, M., Silva, L.C., 2010. Noble gas and carbon isotopic signatures of Cape Verde oceanic carbonatites: implications for carbon provenance. Earth Planet. Sci. Lett. 291, 70–83.
Mattoussi Kort, H., Laridi Ouazaa, N., Kassaa, S., Beji Sassi, A., 2005. Thermal effects of magmatic activity on clay sediments in eastern Tunisia. Mineral Deposit Research: Meeting the Global Challenge 2005, Session 9 999–1001. doi:10.1007/3-540-27946-6_255.
Mauduit, F., 1978. Le volcanisme néogène de la Tunisie continentale. Thèse 3ème cycle. Univ. Paris – Sud (Orsay).
Meddeb, M. N., 1993. Potentialités géothermiques de la Tunisie septentrionale. Thèse de 3ème cycle, Laboratoire Hydrogéologie – Géothermie, Univ. Tunis II F.S.T. et E.N.I.S.
Minissale, A., 2004. Origin, transport and discharge of CO_2 in central Italy. Earth Sci. Rev. 66, 89–141.
Minissale, A., Evans, W.C., Magro, G., Vaselli, O., 1997. Multiple source components in gas manifestations from north-central Italy. Chem. Geol. 142, 175–192.
Minissale, A., Magro, G., Martinelli, G., Vaselli, O., Tassi, F., 2000. Fluid geochemical transect in the Northern Apennines (central-northern Italy): fluid genesis and migration and tectonic implications. Tectonophysics 319, 199–222.
Mlayah, A., Ferreira da Silva, E., Rocha, F., Ben Hamza, Ch., Charef, A., Noronha, F., 2009. The Oued Mellègue: Mining activity, stream sediments and dispersion of base metals in natural environments, North-western Tunisia. J. Geochem. Explor. 102, 27–36.
Mutlu, H., Güleç, N., Hilton, D.R., 2008. Helium–carbon relationships in geothermal fluids of western Anatolia. Turkey. Chem. Geol. 247, 305–321.
Ohmoto, H., Rye, R.O., 1979. Isotopes of sulfur and carbon. In: Barnes, H.L. (Ed.), Geochemistry of Hydrothermal Ore Deposits, pp. 509–567.
Oxburgh, E.R., O'Nions, R.K., Hill, R.I., 1986. Helium isotopes in sedimentary basins. Nature 324, 632–635.
Parello, F., Allard, P., D'Alessandro, W., Federico, C., Jean-Baptiste, P., Catani, O., 2000. Isotope geochemistry of Pantelleria volcanic fluids, Sicily Channel rift: a mantle volatile end-member for volcanism in southern Europe. Earth Planet. Sci. Lett. 180, 325–339.
Parkhurst, D.L., Appelo, C.A.J., 1999. User's guide to PHREEQC (Version 2) — a computer program for speciation, batch-reaction, one-dimensional transport, and inverse geochemical calculations. USGS: Water Resour. Invest. Rep., 99, p. 4259. 310 pp.
Paternoster, M., 2004, Mt. Vulture volcano (Italy): a geochemical contribution to the origin of fluids and to a better definition of its geodynamic setting. PhD dissertation, Università di Palermo.
Perthuisot, V., 1978. Dynamique et pétrogenèse des extrusions triasiques en Tunisie septentrionale. PhD thesis, Ecole Normale Supérieure, Paris, 312 pp.
Pik, R., Marty, B., 2009. Helium isotopic signature of modern and fossil fluids associated with the Corinth rift fault zone (Greece): implication for fault connectivity in the lower crust. Chem. Geol. 266, 67–75.
Polyak, B.G., Tolstikhin, I.N., Kamensky, I.L., Yakovlev, L.E., Marty, B., Cheshko, A.L., 2000. Helium isotopes, tectonics and heat flow in the Northern Caucasus. Geochim. Cosmochim. Acta 64, 1925–1944.
Rouvier, H., 1977. Géologie de l'extrême Nord-tunisien: tectoniques et paléogéographies superposées à l'extrémité orientale de la chaîne Nord-Maghrébine. PhD Thesis, Univ. P.M. Curie, Paris, France, 1000 pp.
Sadki, O., 1998. Etude de systèmes hydrothermaux du Nord de la Tunisie. Géochimie des interactions eaux-roches et circulation hydrothermale. PhD thesis, Laboratoire de géochimie et géologie de l'environnement, Univ. Tunis II F.S.T. et E.N.I.S.
Sano, Y., Williams, S., 1996. Fluxes of mantle and subducted carbon along convergent plate boundaries. Geophys. Res. Lett. 23, 2749–2752.
Stievenard, M., Delmotte, M., Jouzel, J., et al., 1994. Mass spectrometric analysis of water stable isotopes — reconstruction of past climates from polar ice cores. Analusis 22, M21–M24.
Stuart, F.M., Lass-Evans, S., Fitton, J.G., Ellam, R.M., 2003. High ^{3}He/^{4}He ratios in picritic basalts from Baffin Island and role of a mixed reservoir in mantle plumes. Nature 424, 57–59.
Stumm, W., Morgan, J.J., 1996. Aquatic chemistry: chemical equilibria and rates in natural waters. Wiley-Interscience publication.
Tavarnelli, E., Butler, R.W.H., Decandia, F.A., Calamita, F., Grasso, M., Alvarez, W., Renda, P., 2004. Implications of fault reactivation and structural inheritance in the cenozoic tectonic evolution of Italy. IGC: Bollettino della Societa Geologica Italiana, Special Volume, 32, pp. 209–222. 0037–8763.
Tedesco, D., Scarsi, P., 1999. Intensive gas sampling of noble gases and carbon at Vulcano Island (southern Italy). J. Geophys. Res. 104, 10499–10510. doi:10.1029/1998JB 900066.
Trabelsi, R., Zaïri, M., Smida, H., Ben Dhia, H., 2005. Salinization of coastal aquifers : case of the North Sfax Sahel aquifer, Tunisia. C.R. Geosci. 337, 515–524.
Trabelsi, R., Zaïri, M., Ben Dhia, H., 2007. Groundwater salinization of the Sfax superficial aquifer, Tunisia. Hydrogeol. J. 15, 1341–1355.
Trabelsi, R., Kacem, A., Zouari, K., Rozanski, K., 2009. Quantifying regional groundwater flow between Continental Intercalaire and Djeffara aquifers in southern Tunisia using isotope methods. J. Environ. Geol. 58, 171–183.
Wigley, T.M.L., Plummer, L.N., Pearson Jr., F.J., 1978. Mass transfer and carbon isotope evolution in natural waters systems. Geochim. Cosmochim Acta 42, 1117–1139.
Yermani, M., Zouari, K., Michelot, J.L., Mamou, A., Moumni, L., 2003. Geochemical approach to the functioning of the Gafsa North deep aquifer (central Tunisia). Hydrol. Sci. J. J. Sci. Hydrol. 48, 95–108.
Zhang, J., Quay, P.D., Wilbur, D.O., 1995. Carbon isotope fractionation during gas–water exchange and dissolution of CO2. Geochim. Cosmochim. Acta 59, 107–114.
Zouari, K., Chkir, N., Ouda, B., 2003. Palaeoclimatic variation in Maknassi basin (central Tunisia) during Holocene period using pluridisplinary approaches. IAEA Tech. Report, pp. 80–88. Vienna, Austria.